Interference Exploitation Precoding for Multi-Level Modulations: Closed-Form Solutions

Ang Li, *Member, IEEE*, Christos Masouros, *Senior Member, IEEE*, Branka Vucetic, *Life Fellow, IEEE*, Yonghui Li, *Fellow, IEEE*, and A. Lee Swindlehurst, *Fellow, IEEE*

***Abstract*— We study closed-form interference-exploitation precoding for multi-level modulations in the downlink of multi-user multiple-input single-output (MU-MISO) systems. We consider two distinct cases: first, when the number of served users is not larger than the number of transmit antennas at the base station (BS), we mathematically derive the optimal precoding structure based on the Karush-Kuhn-Tucker (KKT) conditions. By formulating the dual problem, the precoding problem is transformed into a pre-scaling operation using quadratic programming (QP) optimization. We further consider the case where the number of served users is larger than the number of transmit antennas at the BS. By employing the pseudo inverse, we show that the optimal solution of the pre-scaling vector is equivalent to a linear combination of the right singular vectors corresponding to zero singular values, and derive the equivalent QP formulation. We also present the condition under which multiplexing more streams than the number of transmit antennas is achievable. For both considered scenarios, we propose a modified iterative algorithm to obtain the optimal precoding matrix, as well as a sub-optimal closed-form precoder. Numerical results validate our derivations on the optimal precoding structures for multi-level modulations, and demonstrate the superiority of interference-exploitation precoding for both scenarios.**

***Index Terms*— MIMO, precoding, constructive interference, Lagrangian, multi-level modulations, closed-form solutions.**

I. Introduction

PRECODING has been widely studied in multi-antenna wireless communication systems to simultaneously support data transmission to multiple users [1]. When the channel state information (CSI) is known at the transmitter side, dirty paper coding (DPC) that subtracts the interference prior to transmission achieves the channel capacity [2]. Despite its promising performance, DPC is generally difficult to implement in practical wireless systems, due to its impractical assumption of an infinite source alphabet and prohibitive complexity. Therefore, sub-optimal approximations of DPC in the form of Tomlinson-Harashima precoding (THP) and vector perturbation (VP) precoding have been proposed in [3] and [4]–[6], respectively. While offering near-optimal performance, both THP and VP approaches are still non-linear precoding methods and include a sphere-search process, which makes their complexity still unfavorable, especially when the number of data streams is large. Accordingly, low-complexity linear precoding methods such as zero-forcing (ZF) [7] and regularized ZF (RZF) [8] have become popular. On the other hand, downlink precoding based on optimization has also received increasing research attention [9]–[15]. Among optimization-based precoding methods, the two most well-known designs are referred to as signal-to-noise-plus-interference ratio (SINR) balancing [9]–[11] and power minimization [12]–[14], where SINR balancing aims to maximize the minimum received SINR subject to a total transmit power constraint [9], [10] or a per-antenna power constraint [11], and power minimization targets minimizing the power consumption at the transmitter side while guaranteeing a minimum SINR at each receiver [13].

For both the closed-form precoding schemes and the optimization-based precoding approaches described above, the CSI at the base station (BS) is exploited to design the precoding strategy that eliminates, avoids or limits interference. The above approaches ignore the fact that the information in the transmitted data symbols themselves can also be exploited in the downlink precoding design on a symbol-by-symbol basis for further performance improvements [16]–[18]. With information about the data symbols and their corresponding constellations, the instantaneous interference can be divided into constructive interference (CI) and destructive interference, as shown in [19]. A modified ZF precoding method was then proposed in [20] to exploit the constructive part of the interference while eliminating the destructive part. A more advanced two-stage interference exploitation precoding was proposed in [21], where the phase of the destructive interference was controlled and further rotated such that the destructive interference becomes constructive. Optimization-based interference exploitation precoding for PSK modulations has been proposed in [22] for the first time in the context of VP precoding, where CI in the form of symbol scaling is proposed.

Manuscript received January 16, 2020; revised May 28, 2020, August 20, 2020, and October 11, 2020; accepted October 12, 2020. Date of publication October 16, 2020; date of current version January 15, 2021. This work was supported in part by the Royal Academy of Engineering, UK, in part by the Engineering and Physical Sciences Research Council (EPSRC) project EP/M014150/1, in part by the Australian Research Council (ARC) under Grant DP150104019 and Grant DP190101988, in part by the ARC Laureate Fellowship under Grant FL160100032, in part by the Science and Technology Program of Shaanxi Province under Grant No. 2019KW-007 and 2020KW-007, and in part by the Fundamental Research Funds for the Central Universities under grant 1191320197. The associate editor coordinating the review of this article and approving it for publication was L. Dai. *(Corresponding author: Ang Li.)*

Ang Li is with the School of Information and Communications Engineering, Faculty of Electronic and Information Engineering, Xi'an Jiaotong University, Xi'an, Shaanxi 710049, China (e-mail: ang.li.2020@xjtu.edu.cn).

Christos Masouros is with the Department of Electronic and Electrical Engineering, University College London, London WC1E 7JE, U.K. (e-mail: c.masouros@ucl.ac.uk).

Branka Vucetic and Yonghui Li are with the School of Electrical and Information Engineering, The University of Sydney, Sydney, NSW 2006, Australia (e-mail: branka.vucetic@sydney.edu.au; yonghui.li@sydney.edu.au).

A. Lee Swindlehurst is with the Department of Electrical Engineering and Computer Science, Henry Samueli School of Engineering, University of California at Irvine, Irvine, CA 92697 USA (e-mail: swindle@uci.edu).

Color versions of one or more of the figures in this article are available online at https://ieeexplore.ieee.org.

Digital Object Identifier 10.1109/TCOMM.2020.3031616

In [23]–[25], CI precoding based on the phase-rotation metric is studied, where it is shown that a relaxed non-strict phase rotation metric is more advantageous compared to the strict phase rotation in [20], [21]. For multi-level modulations such as QAM, CI can be exploited for the outer constellation points, although all the interference for the inner constellation points is considered to be destructive, as discussed in [26]–[28] where a symbol-scaling metric is introduced. Due to the above benefits, CI has been extended to a number of emerging areas in wireless communications [29]–[35]. More recently, it has been revealed in [36] that there exists an optimal structure for the CI precoding for PSK modulations. Based on this result, for the first time some analytical results for CI precoding have been revealed in [37] and [38]. Nevertheless, it is still unclear whether a similar result exists for multi-level modulations such as QAM, since CI precoding for PSK modulations is based on the phase-rotation metric, while the symbol-scaling metric has to be adopted for QAM constellations.

Therefore in this paper, we aim to bridge the gap between the phase-rotation metric and the symbol-scaling metric, based on which closed-form interference exploitation precoding for multi-level modulations is studied, where QAM modulation is considered as a representative example. For clarity, we summarize the main contributions of the paper below:

1) We mathematically prove the equivalency between the symbol-scaling metric and phase-rotation metric for interference exploitation precoding, based on which we construct the optimization problem that maximizes the CI effect of the outer constellation symbols while maintaining the performance of the inner constellation symbols for multi-level modulations.
2) We first study the case where the number of users simultaneously served by the BS is not larger than the number of BS transmit antennas. Using the Lagrangian and KKT conditions, we perform mathematical analysis on the formulated optimization problem, and show that CI precoding for multi-level modulations can ultimately be simplified into a quadratic programming (QP) optimization. We reveal that the optimal precoding matrix can be expressed as a function of the dual variables in closed form. Compared to CI precoding for PSK modulations where the optimization is over a simplex, it is shown that only part of the dual variables need to be constrained as non-negative in the QP formulation for multi-level modulations.
3) We further extend our analysis on CI to the case where the number of served users is larger than the number of transmit antennas at the BS, in which case the exact inverse included in the above analysis becomes inapplicable. In this scenario, we show that interference exploitation precoding may still be feasible. To this end, the more generic pseudo inverse of the channel matrix is employed instead, and an additional constraint is thus introduced in the equivalent optimization. Building upon this, the scaling vector for the constellation symbols is shown to be the non-zero solution of a linear equation set, which is equivalent to a linear combination of the singular vectors corresponding to the zero singular values of the coefficient matrix. Accordingly, the optimization can be transformed into an optimization on the weights for each singular vector, which is further shown to be equivalent to a QP optimization as well. We also present the condition under which multiplexing more streams than the number of transmit antennas based on CI is achievable.
4) For both of the scenarios considered above, we propose an iterative algorithm that is able to obtain the optimal solution of a generic QP optimization problem subject to specific constraints within only a few iterations, where a closed-form update is included in each iteration. Based on the above transformation and algorithm, the optimal precoding matrix can be efficiently obtained. We further develop a sub-optimal closed-form non-iterative CI precoder. Our analysis for multi-level modulations in this paper complements the study on closed-form symbol-level interference exploitation precoding in [32], which is not applicable to multi-level modulations.

Simulation results validate our mathematical derivations and the optimality of the proposed algorithm. Moreover, the superiority of interference exploitation precoding over conventional precoding methods for multi-level modulations is also revealed, especially for the case where the BS simultaneously serves a larger number of users than the number of transmit antennas it has.

The remainder of this paper is organized as follows: Section II introduces the system model and illustrates the connection between the two CI metrics. Section III includes the CI-based optimization problems for multi-level modulations when the number of users is smaller than or equal to the number of BS transmit antennas, and the extension to the scenario when the number of users is larger than the number of BS transmit antennas is studied in Section IV. The modified iterative algorithm and sub-optimal closed-form precoder are presented in Section V. Numerical results are provided in Section VI, and Section VII concludes the paper.

Notation: a, $\mathbf{a}$, and $\mathbf{A}$ denote scalar, column vector and matrix, respectively. $(\cdot)^*$, $(\cdot)^T$, $(\cdot)^H$, $(\cdot)^{-1}$, $(\cdot)^+$ and $\mathrm{rank}\{\cdot\}$ denote conjugate, transposition, conjugate transposition, inverse, pseudo inverse, and rank of a matrix, respectively. $diag(\cdot)$ is the transformation of a column vector into a diagonal matrix, and $\mathrm{vec}(\cdot)$ denotes the vectorization operation. $\mathbf{A}(k,i)$ denotes the entry in the k-row and i-th column of $\mathbf{A}$. $|\cdot|$ denotes the absolute value of a real number or the modulus of a complex number, and $\|\cdot\|_2$ denotes the ℓ_2-norm. $\mathcal{C}^{n\times n}$ and $\mathcal{R}^{n\times n}$ represent the sets of $n\times n$ complex- and real-valued matrices, respectively. $\Re\{\cdot\}$ and $\Im\{\cdot\}$ respectively denote the real and imaginary part of a complex scalar, vector or matrix. $card\{\cdot\}$ denotes the cardinality of a set, and $\otimes$ represents the Kronecker product. j denotes the imaginary unit, $\mathbf{I}_K$ denotes the $K\times K$ identity matrix, and $\mathbf{e}_i$ represents the i-th column of the identity matrix.

II. System Model and Constructive Interference

A. System Model

We study a downlink MU-MISO system, where the BS with N_t transmit antennas is simultaneously communicating with

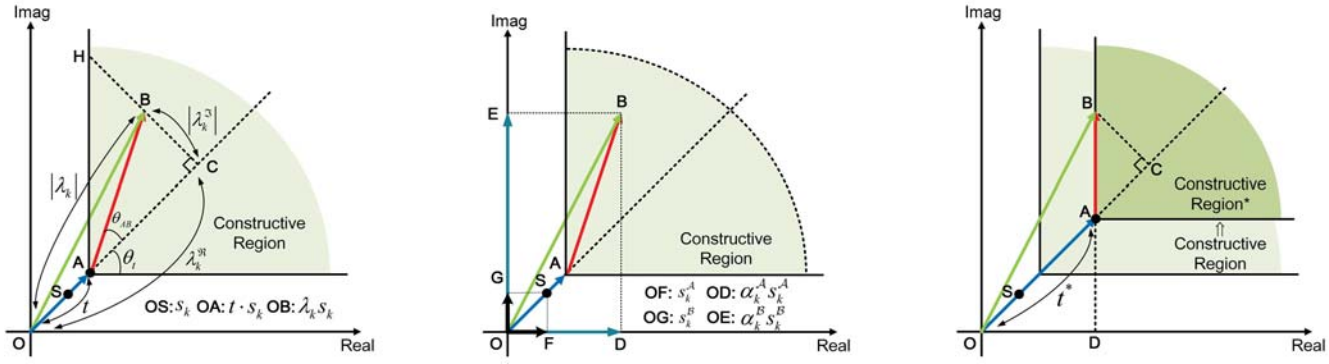

(a) Phase-rotation metric, λ_k: complex scaling factor for s_k

(b) Symbol-scaling metric, $\alpha_k^{\mathcal{A}/\mathcal{B}}$: real scaling factor for $s_k^{\mathcal{A}/\mathcal{B}}$

(c) Illustration for **Lemma 1**

Fig. 1. Symbol-scaling and phase-rotation metric for QPSK constellation, s_k: data symbol.

K single-antenna users in the same time-frequency resource. We separately consider the scenarios of both $K \leq N_t$ and $K > N_t$, and focus on the downlink precoding designs, where perfect CSI is assumed throughout the paper. The data symbol vector is assumed to be from a nominal multi-level modulation constellation where the average amplitude of the constellation points is normalized[1], denoted as $\mathbf{s} = [s_1, s_2, \cdots, s_K]^T \in \mathcal{C}^{K\times 1}$, and the received signal at the k-th user can then be expressed as

$$y_k = \mathbf{h}_k^T \mathbf{W}\mathbf{s} + n_k, \tag{1}$$

where $\mathbf{h}_k \in \mathcal{C}^{N_t\times 1}$ denotes the flat-fading Rayleigh channel vector from user k to the BS with each entry following a standard complex Gaussian distribution, $\mathbf{W} \in \mathcal{C}^{N_t\times K}$ is the precoding matrix, and n_k is the additive Gaussian noise at the receiver with zero mean and variance σ^2. Since we focus on symbol-level precoding, we enforce a symbol-level transmit power constraint at the BS, given by $\|\mathbf{W}\mathbf{s}\|_2^2 \leq p_0$, where p_0 is the total available transmit power.

B. Constructive Interference

CI refers to interference that pushes the received signals away from the detection thresholds corresponding to the transmitted symbols, and thus such interference is beneficial and increases the useful signal power, offering error-rate improvements [16]–[21]. Based on this definition, [23] introduces the concept of the 'constructive region', which is the region in the complex plane into which the interference pushes the received signal such that it is farther away from the decision boundaries shared with other symbols, thus improving the resulting detection performance. As illustrative examples, the 'constructive regions' for a QPSK constellation and a 16QAM constellation are shown in Fig. 1 and Fig. 2, respectively, where the green area denotes the 'constructive region'. By designing the precoding strategy based on the 'constructive region' principle at the BS, the CI-based precoding is shown to offer significant performance improvements for both PSK and QAM signaling, without the need to modify the detection criterion at the receiver side.

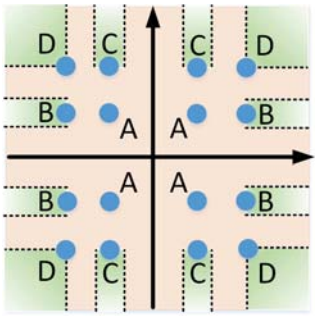

Fig. 2. Constellation point categorization for 16QAM.

C. Equivalency of Two CI Metrics for PSK Modulation

In this section, we demonstrate the equivalency between the symbol-scaling and phase-rotation metrics for CI precoding based on Fig. 1, where we employ QPSK (4QAM) as an example. Our considered problem is to maximize the distance between the 'constructive region' and the detection thresholds such that the CI effect is maximized, subject to the total available transmit power at the BS.

Phase-Rotation Metric: As discussed in Section III-A of [32] and shown in Fig. 1a, the phase-rotation CI metric is obtained by considering the geometry of the phase constraint of the interfered signals. Without loss of generality, we denote $\vec{OS} = s_k$ as a nominal constellation point that is the intended data symbol for user k. We introduce $\vec{OA} = t \cdot s_k$, where $t = \frac{|\vec{OA}|}{|\vec{OS}|}$ represents the distance between the detection thresholds and the 'constructive region', which is the objective to be maximized. We further denote $\vec{OB}$ as the received signal for user k excluding noise, which leads to

$$\vec{OB} = \mathbf{h}_k^T \mathbf{W}\mathbf{s} = \lambda_k s_k, \tag{2}$$

[1]The normalization to obtain nominal constellation points can be expressed as $s_m^{\mathrm{N}} = \frac{s_m^{\mathrm{O}}}{\sqrt{\frac{\sum_{k=1}^{card\{\mathcal{S}\}} |s_k^{\mathrm{O}}|^2}{card\{\mathcal{S}\}}}}$, where s_m^{N} is the normalized constellation point, s_m^{O} is the original constellation point, and $\mathcal{S}$ represents the set of the original constellation points.

where λ_k is a complex auxiliary variable introduced to represent the effect of both the channel and the interference on the data symbol for user k. For $\mathcal{M}$-PSK constellations, following Section III-B of [32], to have the noiseless received signal $\vec{OB}$ located in the 'construcive region' is equivalent to $|\vec{CB}| \leq |\vec{CH}|$ in Fig. 1a, where the node 'H' is the intersection between the decision boundary and the auxiliary line of $\vec{CB}$. With the fact that $\vec{OB} = \vec{OA} + \vec{AC} + \vec{CB}$ and that $\vec{OC}$ and $\vec{CB}$ are perpendicular, we can further obtain that $\vec{AC} = \left(\lambda_k^{\Re} - t\right) s_k$ and $\vec{CB} = \lambda_k^{\Im} s_k$, which leads to

$$\begin{aligned} &|\vec{CB}| \leq |\vec{CH}| \\ &\Rightarrow \frac{|\vec{CB}|}{|\vec{AC}|} \leq \frac{|\vec{CH}|}{|\vec{AC}|} \\ &\Rightarrow \tan\theta_{AB} \leq \tan\theta_t \\ &\Rightarrow \frac{\left|\lambda_k^{\Im}\right|}{\lambda_k^{\Re} - t} \leq \tan\theta_t \\ &\Rightarrow \left(\lambda_k^{\Re} - t\right)\tan\theta_t \geq \left|\lambda_k^{\Im}\right|, \end{aligned} \tag{3}$$

where $\lambda_k^{\Re} = \Re(\lambda_k)$, $\lambda_k^{\Im} = \Im(\lambda_k)$, and $\theta_t = \frac{\pi}{\mathcal{M}}$ for $\mathcal{M}$-PSK constellations.[2] Accordingly, as in [32], the optimization problem based on the phase-rotation CI metric can be formulated as

$$\begin{aligned} \mathcal{P}_1: \quad &\max_{\mathbf{W},\lambda_k,t} \ t \\ &s.t. \ \mathbf{C1}: \mathbf{h}_k^T\mathbf{W}\mathbf{s} = \lambda_k s_k, \ \forall k \in \mathcal{K} \\ &\quad \mathbf{C2}: \ \left(\lambda_k^{\Re} - t\right)\tan\left(\frac{\pi}{\mathcal{M}}\right) \geq \left|\lambda_k^{\Im}\right|, \ \forall k \in \mathcal{K} \\ &\quad \mathbf{C3}: \ \|\mathbf{W}\mathbf{s}\|_2^2 \leq p_0 \end{aligned} \tag{4}$$

where $\mathcal{K} = \{1, 2, \cdots, K\}$. We have enforced a symbol-level power constraint on the precoder, since the exploitation of CI is dependent on the data symbol $\mathbf{s}$, which will also be shown mathematically in the following.

Symbol-Scaling Metric: Following the coordinate transformation approach in the Appendix of [29], the symbol-scaling CI metric performs a signal decomposition along the vectors defining the detection thresholds of the considered constellation point. To be more specific, as shown in Fig. 1b, we first decompose the data symbol along the detection thresholds for each user k as

$$\vec{OS} = \vec{OF} + \vec{OG} \Rightarrow s_k = s_k^{\mathcal{A}} + s_k^{\mathcal{B}}, \tag{5}$$

where $s_k^{\mathcal{A}}$ and $s_k^{\mathcal{B}}$ are the bases that are parallel to the detection thresholds for each specific constellation symbol, as shown in Fig. 1. We refer the interested readers to Section IV-A of [29] for a detailed derivation of the expressions for $s_k^{\mathcal{A}}$ and $s_k^{\mathcal{B}}$ for generic PSK constellations. Specifically for QPSK modulation considered in Fig. 1 as well as QAM modulations in the following part of the paper, we can obtain

$$s_k^{\mathcal{A}} = \Re\{s_k\} = s_k^{\Re}, \ s_k^{\mathcal{B}} = j \cdot \Im\{s_k\} = j \cdot s_k^{\Im}. \tag{6}$$

Following a similar approach to (5), we also decompose the noiseless received signal for each user k along the same detection thresholds, and further introduce two real scalars $\alpha_k^{\mathcal{A}}$ and $\alpha_k^{\mathcal{B}}$ for $s_k^{\mathcal{A}}$ and $s_k^{\mathcal{B}}$, respectively, which leads to

$$\vec{OB} = \vec{OD} + \vec{OE} \Rightarrow \mathbf{h}_k^T\mathbf{W}\mathbf{s} = \alpha_k^{\mathcal{A}} s_k^{\mathcal{A}} + \alpha_k^{\mathcal{B}} s_k^{\mathcal{B}}. \tag{7}$$

It is then observed that the values of these two scalars directly indicate the effect of the CI. Subsequently, the corresponding optimization that maximizes the CI effect based on the symbol-scaling metric can be constructed as

$$\begin{aligned} \mathcal{P}_2: \ &\max_{\mathbf{W},\alpha_k^{\mathcal{U}}} \min_k \ \alpha_k^{\mathcal{U}} \\ &s.t. \ \mathbf{C1}: \mathbf{h}_k^T\mathbf{W}\mathbf{s} = \alpha_k^{\mathcal{A}} s_k^{\mathcal{A}} + \alpha_k^{\mathcal{B}} s_k^{\mathcal{B}}, \ \forall k \in \mathcal{K} \\ &\quad \mathbf{C2}: \ \|\mathbf{W}\mathbf{s}\|_2^2 \leq p_0 \\ &\quad \mathbf{C3}: \mathcal{U} \in \{\mathcal{A}, \mathcal{B}\} \end{aligned} \tag{8}$$

Both of the above optimization problems are convex and can be directly solved with convex optimization tools. Subsequently, based on Fig. 1 and the formulation of the above two optimizations, an important geometrical observation is given, which demonstrates the connection between the symbol-scaling and phase-rotation metric.

Lemma 1: $\mathcal{P}_1$ and $\mathcal{P}_2$ are equivalent optimization problems for generic $\mathcal{M}$-PSK modulations. Moreover, when the optimality of $\mathcal{P}_1$ is achieved, at least one noiseless received signal is located on the boundary of the constructive region, as shown in Fig. 1c. Moreover, the relationship between the minimum value of $\left(\alpha_k^{\mathcal{U}}\right)^*$ in $\mathcal{P}_2$ and the optimal value of t^* in $\mathcal{P}_1$ is expressed as

$$t^* = 2\left(\alpha_k^{\mathcal{U}}\right)^* \left|\left(s_k^{\mathcal{U}}\right)^*\right| \cos\frac{\pi}{\mathcal{M}}, \tag{9}$$

where without loss of generality we have assumed user k achieves the minimum value of α.

Proof: See Appendix A.

Based on the above results, we observe that while the phase-rotation metric and the symbol-scaling metric are both applicable to PSK constellations and are equivalent, only the symbol-scaling metric can be adopted for multi-level QAM constellations. Therefore, the symbol-scaling CI metric is a more generic metric than the phase-rotation metric. In the following section, the symbol-scaling CI metric is employed in the derivation of the optimal precoding matrix for multi-level modulations.

III. CI Precoding for the Case of $K \leq N_t$

In this section, we focus on the common case where $K \leq N_t$, and we consider 16QAM modulation as an example of multi-level modulations. For other multi-level constellations, the problem formulation and the corresponding analysis for the symbol-scaling metric readily follows our derivations in this section in a similar way.

For a generic QAM constellation, we employ the symbol-scaling metric for CI precoding since there does not exist a generic expression for the phase-rotation CI metric for QAM modulations, as shown in Fig. 2 where a 16QAM constellation is depicted as the example. The symbol-scaling metric in (7) can be further expressed in vector form as

$$\mathbf{h}_k^T\mathbf{W}\mathbf{s} = \mathbf{\Omega}_k^T\mathbf{s}_k, \tag{10}$$

[2] $\tan\theta_{AB} \leq \tan\theta_t$ also implies that $\theta_{AB} \leq \theta_t$, which complies with the traditional decoding criterion for PSK signaling.

where we have introduced two column vectors

$$\mathbf{\Omega}_k = \left[\alpha_k^{\mathcal{A}}, \alpha_k^{\mathcal{B}}\right]^T,\ \mathbf{s}_k = \left[s_k^{\mathcal{A}}, s_k^{\mathcal{B}}\right]^T. \tag{11}$$

For QAM constellations, $s_k^{\mathcal{A}}$ and $s_k^{\mathcal{B}}$ are also given by (6). In this work, we consider the interference on the inner constellation points as only destructive, since the interference is less likely to be beneficial for these points. To be more specific, in Fig.2 CI exists for the real part of the constellation point type 'B' and imaginary part of type 'C', while both the real and imaginary part of the constellation point type 'D' can be exploited. Accordingly, following [39], [40] we propose to construct the optimization problem that maximizes the CI effect for the outer constellation points while maintaining the performance for the inner constellation points, given by

$$\begin{aligned}\mathcal{P}_3:\ &\max_{\mathbf{W},\mathbf{\Omega}_k,t}\ t\\ &s.t.\ \mathbf{C1}: \mathbf{h}_k^T\mathbf{W}\mathbf{s} = \mathbf{\Omega}_k^T\mathbf{s}_k,\ \forall k\in\mathcal{K}\\ &\quad\mathbf{C2}: t\le \alpha_m^{\mathcal{O}},\ \forall \alpha_m^{\mathcal{O}}\in\mathcal{O}\\ &\quad\mathbf{C3}: t = \alpha_n^{\mathcal{I}},\ \forall \alpha_n^{\mathcal{I}}\in\mathcal{I}\\ &\quad\mathbf{C4}:\ \|\mathbf{W}\mathbf{s}\|_2^2\le p_0\end{aligned} \tag{12}$$

where the set $\mathcal{O}$ consists of the real scalars corresponding to the real or imaginary part of the outer constellation points that can be scaled, and $\mathcal{I}$ consists of the real scalars corresponding to the real or imaginary part of the constellation points that cannot exploit CI. Accordingly, we obtain

$$\mathcal{O}\cup\mathcal{I} = \left\{\alpha_1^{\mathcal{A}}, \alpha_1^{\mathcal{B}}, \alpha_2^{\mathcal{A}}, \alpha_2^{\mathcal{B}}, \cdots, \alpha_K^{\mathcal{A}}, \alpha_K^{\mathcal{B}}\right\}, \tag{13}$$

and

$$card\left\{\mathcal{O}\right\} + card\left\{\mathcal{I}\right\} = 2K. \tag{14}$$

$\mathcal{P}_3$ is a second-order-cone programming (SOCP) problem, which can be solved via convex optimization tools such as CVX. Specifically, the optimization objective t is equal to the value of $\alpha_k^{\mathcal{I}}$ in the above optimization, which can also be viewed as a scaling factor for the constellation. Moreover, if we further constrain $t = \alpha_m^{\mathcal{O}}$ instead of $t\le\alpha_m^{\mathcal{O}}$ in the above optimization, the solution of the above optimization problem will become a ZF precoder. In the following, we present our derived results for $\mathcal{P}_3$.

Proposition 1: The optimal precoding matrix $\mathbf{W}$ for $\mathcal{P}_3$ as a function of the scaling vector $\mathbf{\Omega}$ is given by

$$\mathbf{W} = \frac{1}{K}\cdot\mathbf{H}^H\left(\mathbf{H}\mathbf{H}^H\right)^{-1}\mathbf{U}diag\left(\mathbf{\Omega}\right)\mathbf{s}_{\mathbf{E}}\hat{\mathbf{s}}^T, \tag{15}$$

where $\hat{\mathbf{s}}$, $\mathbf{\Omega}$, $\mathbf{s}_{\mathbf{E}}$ and $\mathbf{U}$ are given by

$$\begin{aligned}\hat{\mathbf{s}} &= \left[\frac{1}{s_1}, \frac{1}{s_2}, \cdots, \frac{1}{s_K}\right]^T,\ \mathbf{\Omega} = \left[\mathbf{\Omega}_1^T, \mathbf{\Omega}_2^T, \cdots, \mathbf{\Omega}_K^T\right]^T,\\ \mathbf{s}_{\mathbf{E}} &= \left[\mathbf{s}_1^T, \mathbf{s}_2^T, \cdots, \mathbf{s}_K^T\right]^T,\ \mathbf{U} = \mathbf{I}_K\otimes[1,1],\end{aligned} \tag{16}$$

as shown in (72), (74) and (75), respectively.

Proof: See Appendix B.

To proceed, we substitute the expression for $\mathbf{W}$ in (15) into the power constraint, where we note that the power constraint is strictly active when optimality is achieved, as shown in Appendix B, and accordingly we obtain

$$\begin{aligned}&\|\mathbf{W}\mathbf{s}\|_2^2 = p_0\\ &\Rightarrow\ \mathbf{s}^H\mathbf{W}^H\mathbf{W}\mathbf{s} = p_0\\ &\Rightarrow\ \mathbf{s}_{\mathbf{E}}^H diag\left(\mathbf{\Omega}\right)\mathbf{U}^H\left(\mathbf{H}\mathbf{H}^H\right)^{-1}\mathbf{U}diag\left(\mathbf{\Omega}\right)\mathbf{s}_{\mathbf{E}} = p_0\\ &\Rightarrow\ \mathbf{\Omega}^T\underbrace{diag\left(\mathbf{s}_{\mathbf{E}}^H\right)\mathbf{U}^H\left(\mathbf{H}\mathbf{H}^H\right)^{-1}\mathbf{U}diag\left(\mathbf{s}_{\mathbf{E}}\right)}_{\mathbf{T}}\mathbf{\Omega} = p_0\\ &\Rightarrow\ \mathbf{\Omega}^T\mathbf{T}\mathbf{\Omega} = p_0.\end{aligned} \tag{17}$$

Since $\mathbf{T}$ is Hermitian and positive semi-definite, and since each entry in $\mathbf{\Omega}$ is real, (17) can be further transformed into

$$\mathbf{\Omega}^T\mathbf{T}\mathbf{\Omega} = \mathbf{\Omega}^T\Re\left\{\mathbf{T}\right\}\mathbf{\Omega} = \mathbf{\Omega}^T\mathbf{V}\mathbf{\Omega} = p_0, \tag{18}$$

where $\mathbf{V} = \Re\left\{\mathbf{T}\right\}$ is symmetric. With the expression for $\mathbf{W}$ in (15) and the updated power constraint, we are able to construct an equivalent optimization on $\mathbf{\Omega}$, given by

$$\begin{aligned}\mathcal{P}_4:\ &\min_{\mathbf{\Omega},\alpha_m^{\mathcal{O}},\alpha_n^{\mathcal{I}},t}\ -t\\ &s.t.\ \mathbf{C1}: \mathbf{\Omega}^T\mathbf{V}\mathbf{\Omega} - p_0 = 0\\ &\quad\mathbf{C2}: t-\alpha_m^{\mathcal{O}}\le 0,\ \forall\alpha_m^{\mathcal{O}}\in\mathcal{O}\\ &\quad\mathbf{C3}: t-\alpha_n^{\mathcal{I}} = 0,\ \forall\alpha_n^{\mathcal{I}}\in\mathcal{I}\end{aligned} \tag{19}$$

The optimal precoding matrix for the original optimization $\mathcal{P}_3$ is then obtained by substituting the solution of $\mathcal{P}_4$ into (15). Based on $\mathcal{P}_4$, we further derive the final precoding matrix as a function of the dual variables of $\mathcal{P}_4$, as shown below.

Proposition 2: The optimal closed-form precoding matrix $\mathbf{W}$ as a function of the dual vector $\mathbf{u_1}$ in the case of $K\le N_t$ is

$$\begin{aligned}&\mathbf{W}\\ &= \frac{1}{K}\mathbf{H}^H\left(\mathbf{H}\mathbf{H}^H\right)^{-1}\mathbf{U}diag\left(\sqrt{\frac{p_0}{\mathbf{u_1}^T\tilde{\mathbf{V}}^{-1}\mathbf{u_1}}}\mathbf{F}^{-1}\tilde{\mathbf{V}}^{-1}\mathbf{u_1}\right)\mathbf{s}_{\mathbf{E}}\hat{\mathbf{s}}^T,\end{aligned} \tag{20}$$

where $\mathbf{F}^{-1}$ is used to rearrange the obtained $\tilde{\mathbf{\Omega}}$ into the original $\mathbf{\Omega}$, with $\mathbf{F}$ given in (85). $\tilde{\mathbf{V}} = \mathbf{F}\mathbf{V}\mathbf{F}^T$ as in (86), and $\mathbf{u_1}$ is obtained by solving the following QP optimization:

$$\begin{aligned}\mathcal{P}_5:\ &\min_{\mathbf{u_1}}\ \mathbf{u_1}^T\tilde{\mathbf{V}}^{-1}\mathbf{u_1}\\ &s.t.\ \mathbf{C1}: \mathbf{1}^T\mathbf{u_1} - 1 = 0\\ &\quad\mathbf{C2}: \mu_m\ge 0,\ \forall m\in\{1,2,\cdots,card\left\{\mathcal{O}\right\}\}\end{aligned} \tag{21}$$

Proof: See Appendix C.

Compared to the final QP formulation for PSK modulation in [32] that is optimized over a simplex, a key difference for the case of QAM constellations is that the variable vector is no longer on a simplex, and only the dual variables that correspond to the real and imaginary part of the outer constellation points that can exploit CI are constrained to be non-negative, as observed in $\mathcal{P}_5$. We note that both QP formulations for PSK and QAM modulations can be solved by convex optimization tools. However, for the reasons given above, the more efficient simplex method that is generally used for solving QP problems over a simplex and the proposed iterative algorithm in [32] are not directly applicable to such multi-level modulations.

IV. CI Precoding for the Case of $K > N_t$

In this section, we further extend our study to the case where the number of users that the BS simultaneously serves is larger than the number of the transmit antennas at the BS, i.e., $K > N_t$. Specifically, our derivations in this section and the corresponding numerical results show that, by exploiting the information of the channel as well as the data symbols and by judiciously constructing the precoding matrix, CI precoding is able to spatially multiplex more data streams than the number of transmit antennas. Similar to the case of $K \leq N_t$, the subsequent analysis is generic and can be further extended to other multi-level constellations.

When $K > N_t$, the direct inverse included in (15) and (20) becomes infeasible, as the product $\mathbf{H}\mathbf{H}^H$ is rank-deficient. In this case, the more general pseudo inverse instead of the direct matrix inverse is employed [41]. Based on (76), we can now express $\boldsymbol{\Upsilon}$ in the case of $K > N_t$ as

$$\boldsymbol{\Upsilon} = \frac{1}{K} \cdot \left(\mathbf{H}\mathbf{H}^H\right)^+ \mathbf{U} diag\left(\boldsymbol{\Omega}\right) \mathbf{s}_\mathbf{E}, \tag{22}$$

and the obtained precoding matrix $\mathbf{W}$ as

$$\mathbf{W} = \frac{1}{K} \cdot \mathbf{H}^H \left(\mathbf{H}\mathbf{H}^H\right)^+ \mathbf{U} diag\left(\boldsymbol{\Omega}\right) \mathbf{s}_\mathbf{E} \hat{\mathbf{s}}^T. \tag{23}$$

By substituting the expression for the obtained precoding matrix $\mathbf{W}$ into the power constraint, we can similarly obtain

$$\boldsymbol{\Omega}^T diag\left(\mathbf{s}_\mathbf{E}^H\right) \mathbf{U}^H \left(\mathbf{H}\mathbf{H}^H\right)^+ \mathbf{U} diag\left(\mathbf{s}_\mathbf{E}\right) \boldsymbol{\Omega} = p_0. \tag{24}$$

Then, one can easily follow a similar approach to that in Section III to obtain a QP optimization and the corresponding solution. However, we note that the solution obtained by following the above procedure is not a valid one for the case of $K > N_t$, since the inclusion of the pseudo inverse does not guarantee the equality of the original constraint. To be more specific, if we consider $K \leq N_t$ and substitute the obtained precoding matrix in (15) into (73), we obtain

$$\begin{aligned}
&\mathbf{H}\mathbf{W}\mathbf{s} = \mathbf{U} diag\left(\boldsymbol{\Omega}\right) \mathbf{s}_\mathbf{E} \\
&\Rightarrow \mathbf{H} \left[\frac{1}{K} \mathbf{H}^H \left(\mathbf{H}\mathbf{H}^H\right)^{-1} \mathbf{U} diag\left(\boldsymbol{\Omega}\right) \mathbf{s}_\mathbf{E} \hat{\mathbf{s}}^T\right] \mathbf{s} = \mathbf{U} diag\left(\boldsymbol{\Omega}\right) \mathbf{s}_\mathbf{E} \\
&\Rightarrow \mathbf{U} diag\left(\boldsymbol{\Omega}\right) \mathbf{s}_\mathbf{E} = \mathbf{U} diag\left(\boldsymbol{\Omega}\right) \mathbf{s}_\mathbf{E},
\end{aligned} \tag{25}$$

which is always true. This means that the symbol-scaling constraint in (73) is already implicitly included in the power constraint in (17) for the case of $K \leq N_t$. However, in the case of $K > N_t$ where the pseudo inverse is employed, the above equality may not hold and simply following the approach for $K \leq N_t$ will lead to an erroneous solution. Therefore, the following additional constraint is further required in the case of $K > N_t$ to obtain a valid and correct solution:

$$\begin{aligned}
&\mathbf{H} \left[\frac{1}{K} \mathbf{H}^H \left(\mathbf{H}\mathbf{H}^H\right)^+ \mathbf{U} diag\left(\boldsymbol{\Omega}\right) \mathbf{s}_\mathbf{E} \hat{\mathbf{s}}^T\right] \mathbf{s} \\
&\quad = \mathbf{U} diag\left(\boldsymbol{\Omega}\right) \mathbf{s}_\mathbf{E} \\
&\quad \Rightarrow \ \mathbf{H}\mathbf{H}^H \left(\mathbf{H}\mathbf{H}^H\right)^+ \mathbf{U} diag\left(\boldsymbol{\Omega}\right) \mathbf{s}_\mathbf{E} = \mathbf{U} diag\left(\boldsymbol{\Omega}\right) \mathbf{s}_\mathbf{E} \\
&\quad \Rightarrow \left[\mathbf{H}\mathbf{H}^H \left(\mathbf{H}\mathbf{H}^H\right)^+ - \mathbf{I}_K\right] \mathbf{U} diag\left(\boldsymbol{\Omega}\right) \mathbf{s}_\mathbf{E} = \mathbf{0} \\
&\quad \Rightarrow \underbrace{\left[\mathbf{H}\mathbf{H}^H \left(\mathbf{H}\mathbf{H}^H\right)^+ - \mathbf{I}_K\right] \mathbf{U} diag\left(\mathbf{s}_\mathbf{E}\right)}_{\mathbf{P}} \boldsymbol{\Omega} = \mathbf{0},
\end{aligned} \tag{26}$$

where the matrix $\mathbf{P}$ satifies the following property.

Lemma 2: The rank of the coefficient matrix $\mathbf{P}$ is $(K - N_t)$ with probability 1.

Proof: See Appendix D.

Based on (26), while it is obvious that $\boldsymbol{\Omega} = \mathbf{0}$ can be the solution of the above equation set, this is not a valid solution to the original CI problem. Therefore, this additional constraint is equivalent to having non-zero solutions $\boldsymbol{\Omega}$ for the linear equation $\mathbf{P}\boldsymbol{\Omega} = \mathbf{0}$. Noting that $\mathbf{P}$ is complex while $\boldsymbol{\Omega}$ is constrained to be real, we expand $\mathbf{P} \in \mathcal{C}^{K \times 2K}$ into its real equivalent $\mathbf{P}_\mathbf{E} \in \mathcal{R}^{2K \times 2K}$, given by

$$\mathbf{P}_\mathbf{E} = \begin{bmatrix} \Re\left(\mathbf{P}\right) \\ \Im\left(\mathbf{P}\right) \end{bmatrix}, \tag{27}$$

and based on **Lemma 2** we obtain that $\mathrm{rank}\{\mathbf{P}_\mathbf{E}\} = 2\left(K - N_t\right)$, given that $\mathbf{H}$ is complex and full-rank and that $\mathbf{s}$ is drawn from a complex QAM constellation. We further express the singular value decomposition (SVD) of $\mathbf{P}_\mathbf{E}$ as

$$\mathbf{P}_\mathbf{E} = \mathbf{S}\boldsymbol{\Sigma}\hat{\mathbf{D}}^H, \tag{28}$$

where $\hat{\mathbf{D}} = \left[\hat{\mathbf{d}}_1, \hat{\mathbf{d}}_2, \cdots, \hat{\mathbf{d}}_{2K}\right]$ is the matrix that consists of the right singular vectors. Thus, the non-zero solution $\boldsymbol{\Omega}$ is in the null space of $\mathbf{P}_\mathbf{E}$, and can be expressed as a linear combination of the right singular vectors that correspond to zero singular values:

$$\begin{aligned}
\boldsymbol{\Omega} &= \sum_{n=1}^{2K - \mathrm{rank}\{\mathbf{P}_\mathbf{E}\}} \beta_n \cdot \hat{\mathbf{d}}_{\mathrm{rank}\{\mathbf{P}_\mathbf{E}\}+n} \\
&= \sum_{n=1}^{2N_t} \beta_n \cdot \hat{\mathbf{d}}_{2(K-N_t)+n} \\
&= \mathbf{D}\boldsymbol{\beta},
\end{aligned} \tag{29}$$

where each β_n is real and represents the weight for the corresponding singular vector, $\boldsymbol{\beta} = [\beta_1, \beta_2, \cdots, \beta_{2N_t}]^T$, and $\mathbf{D} \in \mathcal{R}^{2K \times 2N_t}$ consists of the right singular vectors of $\mathbf{P}_\mathbf{E}$ that correspond to the zero singular values, given by

$$\begin{aligned}
\mathbf{D} &= \left[\hat{\mathbf{d}}_{2(K-N_t)+1}, \hat{\mathbf{d}}_{2(K-N_t)+2}, \cdots, \hat{\mathbf{d}}_{2K}\right] \\
&= \left[\mathbf{d}_1, \mathbf{d}_2, \cdots, \mathbf{d}_{2K}\right]^T,
\end{aligned} \tag{30}$$

where each $\mathbf{d}_k^T$ then represents the k-th row of $\mathbf{D}$. By substituting the expression for $\mathbf{D}$ into the power constraint in (24), we further obtain

$$\boldsymbol{\beta}^T \underbrace{\mathbf{D}^T diag\left(\mathbf{s}_\mathbf{E}^H\right) \mathbf{U}^H \left(\mathbf{H}\mathbf{H}^H\right)^+ \mathbf{U} diag\left(\mathbf{s}_\mathbf{E}\right) \mathbf{D}}_{\mathbf{X}} \boldsymbol{\beta} = p_0, \tag{31}$$

which is the valid power constraint for the case of $K > N_t$. The reason for the key difference in the power constraint between the case of $K \leq N_t$ and $K > N_t$ is that, while the symbol-scaling constraint in (10) is automatically satisfied by (17) for the case of $K \leq N_t$, it may not hold for the case of $K > N_t$ and therefore the expression for $\boldsymbol{\Omega}$ in (29) is required to guarantee the symbol-scaling constraint (10) is met for the original CI precoding.

Based on the above analysis, we have obtained an expression for $\boldsymbol{\Omega}$ as a function of $\boldsymbol{\beta}$, as shown in (29). Accordingly, we have the following result in the case of $K > N_t$.

Proposition 3: The optimal closed-form precoding matrix in the case of $K > N_t$ can be expressed as a function of the dual vector $\mathbf{u}_2$, as shown in (33), shown at the bottom of the page, where $\mathbf{u}_2$ is obtained by solving the following QP problem:

$$\begin{aligned}\mathcal{P}_6: \ &\min_{\mathbf{u_2}} \ \mathbf{u_2}^T \left(\mathbf{F}\mathbf{D}\mathbf{Y}^{-1}\mathbf{D}^T\mathbf{F}^T\right)\mathbf{u_2} \\ &s.t. \ \mathbf{C1}: \mathbf{1}^T\mathbf{u_2} - 1 = 0 \\ &\quad \mathbf{C2}: \tilde{\mu}_m \geq 0, \ \forall m \in \{1, 2, \cdots, card\{\mathcal{O}\}\} \end{aligned} \quad (32)$$

where $\mathbf{Y} = \Re(\mathbf{X})$.

Proof: See Appendix E.

Finally, we discuss the condition under which multiplexing $K > N_t$ streams is achievable. Based on the above analysis, we can obtain an expression for the optimal t in the case of $K > N_t$ as

$$t^* = \min_k \ \mathbf{d}_k^T\boldsymbol{\beta}, \ \forall k \in \{1, 2, \cdots, 2K\}. \quad (34)$$

Accordingly, we obtain that if $t^* > 0$, the obtained scaling vector $\boldsymbol{\Omega}$ and the resulting precoding matrix are valid solutions to the original CI precoding problem. Otherwise if $t^* < 0$, each data symbol will be scaled to the other 3 quarters of the constellation, which will lead to erroneous demodulation. Therefore, the condition

$$\min_k \left(\mathbf{d}_k^T\boldsymbol{\beta}\right) > 0 \quad (35)$$

determines when multiplexing $K > N_t$ users is achievable.

V. A Generic Iterative Algorithm for Multi-Level Modulations

Since not all the variables are constrained to be non-negative in the QP formulation for multi-level modulations, as observed in $\mathcal{P}_5$ and $\mathcal{P}_6$, the iterative algorithm designed for PSK modulation does not directly apply to the case of multi-level constellations. Therefore in this section, we propose an iterative algorithm for a generic QP optimization, as an extension of the algorithm designed only for PSK modulations. Specifically, we focus on the following generic QP optimization

$$\begin{aligned}\mathcal{P}_7: \ &\min_{\mathbf{u}} \ \mathbf{u}^T\mathbf{Q}\mathbf{u} \\ &s.t. \ \mathbf{C1}: \mathbf{1}^T\mathbf{u} - 1 = 0 \\ &\quad \mathbf{C2}: \mu_n \geq 0, \ \forall n \in \{1, 2, \cdots, N\} \end{aligned} \quad (36)$$

where $\mathbf{Q}$ is symmetric and positive definite, $\mathbf{u} = [\mu_1, \mu_2, \cdots, \mu_M]^T \in \mathcal{C}^{M\times 1}$ and $N < M$. The above QP formulation can be regarded as a generalization of the QP formulation for both the case of $K \leq N_t$ and $K > N_t$ considered in this paper, as well as for PSK modulations if $M = N$. We express the Lagrangian of $\mathcal{P}_7$ as

$$\begin{aligned}\mathcal{L}(\mathbf{u}, q_0, q_n) &= \mathbf{u}^T\mathbf{Q}\mathbf{u} + q_0\left(\mathbf{1}^T\mathbf{u} - 1\right) - \sum_{n=1}^{N} q_n\mu_n \\ &= \mathbf{u}^T\mathbf{Q}\mathbf{u} + q_0 \cdot \mathbf{1}^T\mathbf{u} - \mathbf{q}_\mathbf{E}^T\mathbf{u} - q_0, \end{aligned} \quad (37)$$

where $\mathbf{q_E} \in \mathcal{C}^{M\times 1}$ is given by

$$\mathbf{q_E} = [q_1, q_2, \cdots, q_N, 0, \cdots, 0]^T = \left[\mathbf{q}^T, \mathbf{0}^{1\times(M-N)}\right]^T. \quad (38)$$

The corresponding KKT conditions can be obtained as

$$\frac{\partial\mathcal{L}}{\partial\mathbf{u}} = 2\mathbf{Q}\mathbf{u} + q_0 \cdot \mathbf{1} - \mathbf{q_E} = 0 \quad (39a)$$

$$\mathbf{1}^T\mathbf{u} - 1 = 0 \quad (39b)$$

$$q_n\mu_n = 0, \ \forall n \in \{1, 2, \cdots, N\} \quad (39c)$$

Based on the above, we obtain the expression for $\mathbf{u}$ as

$$\mathbf{u} = \frac{1}{2}\mathbf{Q}^{-1}\left(\mathbf{q_E} - q_0 \cdot \mathbf{1}\right) = \frac{1}{2}\left(\mathbf{Q}^{-1}\mathbf{q_E} - q_0 \cdot \mathbf{a}\right), \quad (40)$$

where $\mathbf{a} = \mathbf{Q}^{-1}\mathbf{1}$ represents the sum of all the columns of $\mathbf{Q}^{-1}$. By substituting the expression for $\mathbf{u}$ into (39b), we obtain q_0 as a function of $\mathbf{q_E}$:

$$\begin{aligned}&\mathbf{1}^T\left[\frac{1}{2}\left(\mathbf{Q}^{-1}\mathbf{q_E} - q_0 \cdot \mathbf{a}\right)\right] - 1 = 0 \\ &\Rightarrow \frac{1}{2} \cdot \mathbf{1}^T\mathbf{Q}^{-1}\mathbf{q_E} - \frac{q_0}{2} \cdot \mathbf{1}^T\mathbf{a} - 1 = 0 \\ &\Rightarrow q_0 = \frac{\mathbf{1}^T\mathbf{Q}^{-1}\mathbf{q_E} - 2}{\mathbf{1}^T\mathbf{a}} \\ &\Rightarrow q_0 = \frac{\mathbf{b}\mathbf{q_E} - 2}{c}, \end{aligned} \quad (41)$$

where $c = \mathbf{1}^T\mathbf{a}$ denotes the sum of all the entries in $\mathbf{Q}^{-1}$, and $\mathbf{b}^T = \mathbf{1}^T\mathbf{Q}^{-1}$ is the sum of all the rows of $\mathbf{Q}^{-1}$. Due to the symmetry of $\mathbf{Q}$, we further obtain $\mathbf{b} = \mathbf{a}^T$. By substituting q_0 into (40), we further obtain $\mathbf{u}$ as a function of $\mathbf{q_E}$:

$$\begin{aligned}\mathbf{u} &= \frac{1}{2} \cdot \mathbf{Q}^{-1}\mathbf{q_E} - \frac{\mathbf{a}}{2} \cdot \frac{\mathbf{b}\mathbf{q_E} - 2}{c} \\ &= \frac{1}{2} \cdot \mathbf{Q}^{-1}\mathbf{q_E} - \frac{\mathbf{a}\mathbf{b}\mathbf{q_E}}{2c} + \frac{\mathbf{a}}{c} \\ &= \frac{1}{2}\left(\mathbf{Q}^{-1} - \boldsymbol{\Phi}\right)\mathbf{q_E} + \frac{\mathbf{a}}{c}, \end{aligned} \quad (42)$$

where $\boldsymbol{\Phi} = \frac{\mathbf{a}\mathbf{b}}{c}$. Based on the derived expression for $\mathbf{u}$, the following two lemmas are presented.

Lemma 3: When $K \leq N_t$, symbol-level ZF precoding can be viewed as a special case of CI-based precoding, when all the dual variables are forced to be zero.

Proof: See Appendix F.

Lemma 4: The solution for $\mathbf{u}$ in (42) automatically satisfies $\mathbf{1}^T\mathbf{u} - 1 = 0$, irrespective of the value of $\mathbf{q_E}$.

Proof: See Appendix G.

Following **Lemma 4**, $\mathcal{P}_7$ is equivalent to the following optimization problem:

$$\begin{aligned}\mathcal{P}_8: \ &\text{find } \mathbf{q_E} \\ &s.t. \ \mathbf{C1}: \mathbf{u} = \frac{1}{2}\left(\mathbf{Q}^{-1} - \boldsymbol{\Phi}\right)\mathbf{q_E} + \frac{\mathbf{a}}{c} \\ &\quad \mathbf{C2}: \mu_n q_n = 0, \ \mu_n \geq 0, \ q_n \geq 0, \ \forall n \in \{1, 2, \cdots, N\} \end{aligned} \quad (43)$$

$$\mathbf{W} = \frac{1}{K} \cdot \mathbf{H}^H\left(\mathbf{H}\mathbf{H}^H\right)^+\mathbf{U}diag\left(\sqrt{\frac{p_0}{\mathbf{u_2}^T\mathbf{F}\mathbf{D}\mathbf{Y}^{-1}\mathbf{D}^T\mathbf{F}^T\mathbf{u_2}}} \cdot \mathbf{D}\mathbf{Y}^{-1}\mathbf{D}^T\mathbf{F}^T\mathbf{u_2}\right)\mathbf{s_E}\hat{\mathbf{s}}^T, \quad (33)$$

Based on the expression for $\mathbf{q_E}$ in (38), we decompose $\mathbf{Q}^{-1}$ and $\mathbf{\Phi}$ into 2 blocks, given by

$$\mathbf{Q}^{-1} = \left[\begin{array}{cc}\mathbf{Q_1} & \mathbf{Q_2}\end{array}\right], \ \mathbf{\Phi} = \left[\begin{array}{cc}\mathbf{\Phi_1} & \mathbf{\Phi_2}\end{array}\right], \tag{44}$$

where the dimension of both $\mathbf{Q_1}$ and $\mathbf{\Phi_1}$ is $M \times N$. Subsequently, $\mathbf{u}$ in (42) can be further simplified and expressed as a function of $\mathbf{q}$, given by

$$\begin{aligned}\mathbf{u} &= \frac{1}{2}\left(\mathbf{Q_1} - \mathbf{\Phi_1}\right)\mathbf{q} + \frac{\mathbf{a}}{c} \\ &= \frac{1}{2}\mathbf{G}\mathbf{q} + \frac{\mathbf{a}}{c}.\end{aligned} \tag{45}$$

Moreover, noting that only part of the entries in $\mathbf{u}$ are constrained to be non-negative in the original optimization $\mathcal{P}_7$, we further decompose $\mathbf{u}$, $\mathbf{Q_1}$, $\mathbf{\Phi_1}$ and $\mathbf{a}$ into

$$\mathbf{u} = \begin{bmatrix}\mathbf{u_A} \\ \mathbf{u_B}\end{bmatrix}, \quad \mathbf{G} = \begin{bmatrix}\mathbf{G_A} \\ \mathbf{G_B}\end{bmatrix}, \ \mathbf{a} = \begin{bmatrix}\mathbf{a_A} \\ \mathbf{a_B}\end{bmatrix}, \tag{46}$$

where $\mathbf{u_A} \in \mathcal{C}^{N\times 1}$ consists of non-negative dual variables and can be expressed as

$$\mathbf{u_A} = \frac{1}{2}\mathbf{G_A}\mathbf{q} + \frac{\mathbf{a_A}}{c}. \tag{47}$$

Based on the above transformation and the iterative algorithm proposed in Section V of [32], we propose an iterative algorithm for the generic QP formulation in $\mathcal{P}_7$, given in Algorithm 1. The proposed algorithm is applicable to both scenarios $K \leq N_t$ and $K > N_t$, by constructing the coefficient matrix $\mathbf{Q}$ as $\mathbf{Q} = \tilde{\mathbf{V}}^{-1}$ in (21) and as $\mathbf{Q} = \mathbf{F}\mathbf{D}\mathbf{Y}^{-1}\mathbf{D}^T\mathbf{F}^T$ in (32), respectively.

A. The Sub-Optimal Closed-Form Precoder

While the algorithm proposed above includes a closed-form expression within each iteration, it is still an iterative algorithm in nature. Therefore, we further propose a closed-form precoder that achieves sub-optimal performance, for both scenarios considered in this paper. The proposition of this sub-optimal precoder is based on the observation that there is at most only one entry in $\mathbf{q_E}$ that is non-zero for some of the channel realizations.

It has been demonstrated in **Lemma 3** that the CI precoder will reduce to the ZF precoder when $\mathbf{q_E}$ is a zero vector. Therefore in this section, we focus on the scenario where only one entry in $\mathbf{q_E}$ is non-zero. This corresponds to the case where only one entry in $\mathbf{a_A}$ is negative, which violates the constraints in $\mathcal{P}_7$ if $\mathbf{q_E}$ is a zero vector. Without loss of generality, we assume $d = \min\left(\mathbf{a_A}\right) < 0$ and k is the corresponding index, i.e., $d = \mathbf{a_A}\left(k\right) = \min\left(\mathbf{a_A}\right)$. We can then obtain $\mu_k = 0$ and $q_k \neq 0$ based on $\mathcal{P}_8$. Subsequently, based on (47), we can further express

$$\begin{aligned}\bigcap \mu_k \ &= \ \mathbf{u_A}\left(k\right) = \frac{1}{2}\mathbf{G_A}\left(k,k\right)q_k + \frac{\mathbf{a_A}\left(k\right)}{c} = 0 \\ &\Rightarrow \ q_k = -\frac{2\mathbf{a_A}\left(k\right)}{c\mathbf{G_A}\left(k,k\right)},\end{aligned} \tag{48}$$

where $\mathbf{G_A}\left(k,k\right)$ denotes the entry in the k-th row and k-th column of $\mathbf{G_A}$. (48) is based on the assumption that only one entry in $\mathbf{q}$ is non-zero, otherwise the complementary slackness condition will not be satisfied. By decomposing $\mathbf{G_A} = [\mathbf{g}_1, \mathbf{g}_2, \cdots, \mathbf{g}_N]$ where $\mathbf{g}_k$ is the k-th column of $\mathbf{G_A}$ and by introducing $e = \mathbf{G_A}\left(k,k\right)$, the resulting sub-optimal solution for $\mathbf{u}$ can be obtained based on (45), given by

$$\begin{aligned}\mathbf{u} &= \frac{1}{2}\mathbf{g}_k \cdot \left[-\frac{2\mathbf{a_A}\left(k\right)}{c\mathbf{G_A}\left(k,k\right)}\right] + \frac{\mathbf{a}}{c} \\ &= -\frac{\mathbf{a_A}\left(k\right)\cdot\mathbf{g}_k - \mathbf{G_A}\left(k,k\right)\cdot\mathbf{a}}{c\mathbf{G_A}\left(k,k\right)} \\ &= -\frac{d\cdot\mathbf{g}_k - e\cdot\mathbf{a}}{ce}.\end{aligned} \tag{49}$$

Based on the obtained sub-optimal $\mathbf{u}$ in (49) and by substituting $\mathbf{Q} = \tilde{\mathbf{V}}^{-1}$, we are able to express the sub-optimal closed-form CI precoder for the case of $K \leq N_t$ in (50), as shown at the bottom of the next page. The sub-optimal closed-form CI precoder for the case of $K > N_t$ can be obtained in a similar form and is therefore omitted for brevity.

Algorithm 1 Proposed Algorithm for a Generic QP Optimization $\mathcal{P}_{13}$

input : $\mathbf{Q}$
output : $\mathbf{u}^*$
$\mathbf{i} = [\,]$, $I = \text{length}\left(\mathbf{i}\right)$, $\mathbf{N} = [1]$, $n = 1$, and $\text{Iter} = 0$;
Calculate $\mathbf{a} = \mathbf{Q}^{-1}\mathbf{1}$, $c = \mathbf{1}^T\mathbf{a}$;
Obtain $\mathbf{G}$ in (45), $\mathbf{u} = \frac{\mathbf{a}}{c}$ and $\mathbf{u_A} = \frac{\mathbf{a_A}}{c}$;
if $\min\left(\mathbf{u_A}\right) < 0$ **then**
  Set $\mathbf{u}^* = \mathbf{u}$;
else
  while $\min\left(\mathbf{u_A}\right) < 0$ and $\text{Iter} < \text{Iter}_{\max}$ **do**
    $\mathbf{d} = \text{sort}\left(\mathbf{u_A}\right)$;
    find $\mu_k = d_n$; Stack $\mathbf{N} = \left[\mathbf{N}\ 1\right]$, $\mathbf{i} = \left[\mathbf{i}\ k\right]$;
    Update I;
    Construct $\mathbf{Z} = \begin{bmatrix}\mathbf{G}\left(i_1,i_1\right) & \cdots & \mathbf{G}\left(i_1,i_I\right) \\ \vdots & \ddots & \vdots \\ \mathbf{G}\left(i_I,i_1\right) & \cdots & \mathbf{G}\left(i_I,i_I\right)\end{bmatrix}$;
    Set $\tilde{\mathbf{a}}_\mathbf{A} = \left[\mathbf{a_A}\left(i_1\right), \mathbf{a_A}\left(i_2\right), \cdots, \mathbf{a_A}\left(i_I\right)\right]^T$;
    Calculate $\tilde{\mathbf{q}} = -\frac{2}{c}\cdot\mathbf{Z}^{-1}\tilde{\mathbf{a}}_\mathbf{A}$;
    if $\min\left(\tilde{\mathbf{q}}\right) \geq 0$ **then**
      Update $\mathbf{u}$ and $\mathbf{u_A}$;
      $n = 1$;
    else
      find $q_k = \min\left(\tilde{\mathbf{q}}\right)$ and $i_m = k$;
      Set $\mathbf{i} = \mathbf{i}\left(1:m\right)$ and $\mathbf{N} = \mathbf{N}\left(1:m\right)$;
      Update I, $\mathbf{Z}$, $\tilde{\mathbf{a}}$, $\tilde{\mathbf{q}}$, $\mathbf{u}$, and $\mathbf{u_A}$;
      Update $\mathbf{N}\left(m\right) \leftarrow \mathbf{N}\left(m\right) + 1$;
      Update $n = \mathbf{N}\left(m\right)$;
    end if
    $\text{Iter} \leftarrow \text{Iter} + 1$;
  end while
  Obtain $\mathbf{u}^* = \mathbf{u}$;
end if

VI. Numerical Results

In this section, the numerical results of the proposed schemes are presented and compared with traditional CI precoding using Monte Carlo simulations. In each plot,

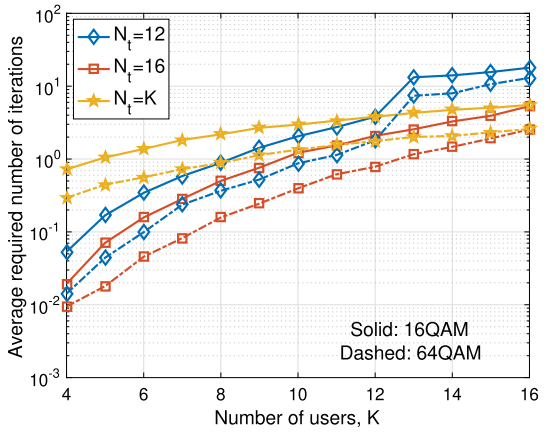

Fig. 3. Average required number of iterations v.s. number of users K, $N_t = 12$, $N_t = 16$ and $N_t = K$, 2000 trials.

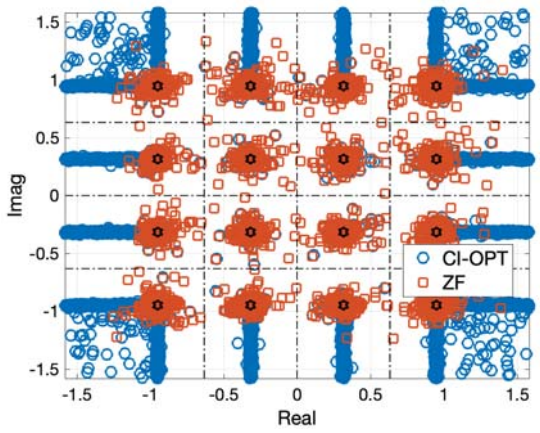

Fig. 4. Received constellation, 16QAM, $N_t = K = 8$, SNR=50dB.

we assume the total transmit power is $p_0 = 1$, and the transmit SNR per antenna is thus $\rho = 1/\sigma^2$. For the case of $K \leq N_t$, we compare our proposed iterative schemes with symbol-level ZF precoding, RZF precoding, and optimization-based CI precoding approach. For the case of $K > N_t$, we compare our proposed iterative algorithm with RZF precoding and the optimization-based CI precoding method. Both 16QAM and 64QAM modulations are considered in the numerical results.

The following abbreviations are used throughout this section:

1) 'ZF': traditional ZF scheme with symbol-level power normalization for $K \leq N_t$. The ZF precoded signals are $\mathbf{x}_{\text{ZF}} = \frac{\sqrt{p_0}}{f_{\text{ZF}}} \cdot \mathbf{H}^H \left(\mathbf{H}\mathbf{H}^H\right)^{-1} \mathbf{s}$, where $f_{\text{ZF}} = \left\| \mathbf{H}^H \left(\mathbf{H}\mathbf{H}^H\right)^{-1} \mathbf{s} \right\|_2$ [7];
2) 'RZF': traditional RZF scheme with symbol-level power normalization for both $K \leq N_t$ and $K > N_t$. The RZF precoded signals are $\mathbf{x}_{\text{RZF}} = \frac{\sqrt{p_0}}{f_{\text{RZF}}} \cdot \mathbf{H}^H \left(\mathbf{H}\mathbf{H}^H + \frac{K}{\sigma^2} \cdot \mathbf{I}\right)^{-1} \mathbf{s}$, where $f_{\text{RZF}} = \left\| \mathbf{H}^H \left(\mathbf{H}\mathbf{H}^H + \frac{K}{\sigma^2} \cdot \mathbf{I}\right)^{-1} \mathbf{s} \right\|_2$ [8];
3) 'CI-OPT': traditional optimization-based CI precoding based on $\mathcal{P}_3$;
4) 'CI-Iterative': iterative CI precoding scheme based on Algorithm 1;
5) 'CI-CF': sub-optimal closed-form CI precoder introduced in Section V-A.

Before we present the detailed bit error rate (BER) results, in Fig. 3 we first show the average number of iterations required for the proposed algorithm to achieve the optimality with an increasing number of users, where we consider the case of '$N_t = 12$' and '$N_t = 16$', as well as the case of '$N_t = K$'. Generally, we observe that the required number of iterations increases with the number of users, since there is a higher possibility that more entries in $\mathbf{a}_{\mathbf{A}}$ are negative. Comparing the result of '$N_t = 16$' with '$N_t = K$', we observe that the required number of iterations becomes smaller when $K < N_t$. This is because the channel becomes closer to orthogonal when $(N_t - K)$ is larger, in which case it is very likely that the optimal CI solution will reduce to symbol-level ZF precoding, and the resulting required number of iterations is 0. Moreover, for the case of '$N_t = 12$', we observe a significant increase in the number of iterations when $K \geq 13$, which is because the scenario is shifted from '$K \leq N_t$' to '$K > N_t$', where the formulation $\mathbf{Q}$ in Algorithm 1 follows (32) instead of (21). Comparing the results of 16QAM with 64QAM, it is also observed that the required number of iterations for 64QAM is smaller than that for 16QAM, as the optimal CI precoding is more likely to be a ZF precoder for 64QAM. In the following, we present the BER results for the scenarios of both $K \leq N_t$ and $K > N_t$. For the case of $K \leq N_t$, we focus on the symmetric case $K = N_t$ which is the most challenging.

A. $K \leq N_t$

Fig. 4 compares the received constellation of CI precoding with traditional ZF precoding for 16QAM modulation, where $K = N_t = 8$. As can be observed, the received noisy data symbols of ZF precoding are located near the nominal constellation points, which comply with the idea of ZF which fully removes the multi-user interference. As for CI precoding, we observe that the received data symbols are pushed away from the decision boundaries and coincide with Fig. 2, which validates the effectiveness of CI precoding.

Fig. 5 presents the BER performance for different precoding schemes with 16QAM modulation, where $K = N_t = 8$. As can be observed, the interference-exploitation precoding

$$\mathbf{W} = \begin{cases} \frac{1}{K} \cdot \mathbf{H}^H \left(\mathbf{H}\mathbf{H}^H\right)^{-1} \mathbf{U} \cdot diag\left\{ \sqrt{\frac{p_0}{\mathbf{1}^T \tilde{\mathbf{V}} \mathbf{1}}} \cdot \mathbf{F}^{-1} \mathbf{1} \right\} \mathbf{s}_{\mathbf{E}} \hat{\mathbf{s}}^T, & \text{if } d \geq 0 \\ \frac{1}{K} \cdot \mathbf{H}^H \left(\mathbf{H}\mathbf{H}^H\right)^{-1} \mathbf{U} \cdot diag\left\{ \sqrt{\frac{p_0 e^2}{\left(d \cdot \mathbf{g}_k^T + e \cdot \mathbf{1}^T \tilde{\mathbf{V}}\right)\left(d \cdot \tilde{\mathbf{V}}^{-1} \mathbf{g}_k + e \cdot \mathbf{1}\right)}} \mathbf{F}^{-1} \left(d \cdot \tilde{\mathbf{V}}^{-1} \mathbf{g}_k + e \cdot \mathbf{1}\right) \right\} \mathbf{s}_{\mathbf{E}} \hat{\mathbf{s}}^T, & \text{if } d < 0 \end{cases} \tag{50}$$

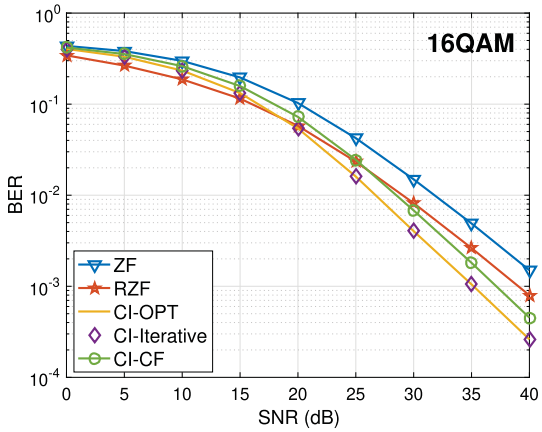

Fig. 5. Uncoded BER v.s. SNR, 16QAM, $N_t = K = 8$.

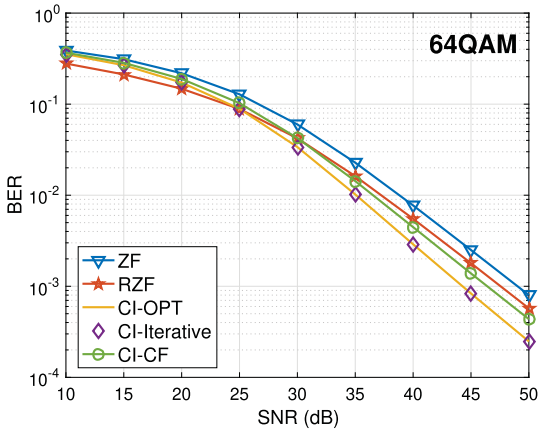

Fig. 7. Uncoded BER v.s. SNR, 64QAM, $N_t = K = 12$.

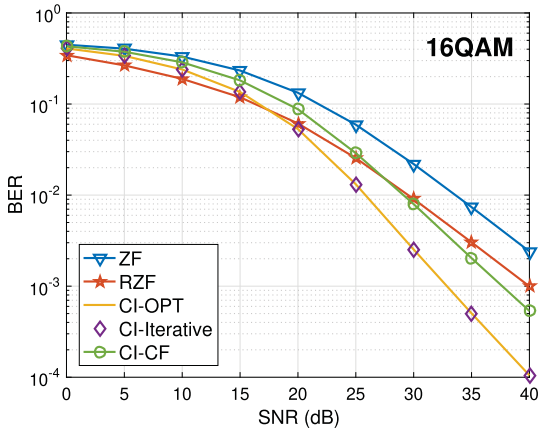

Fig. 6. Uncoded BER v.s. SNR, 16QAM, $N_t = K = 12$.

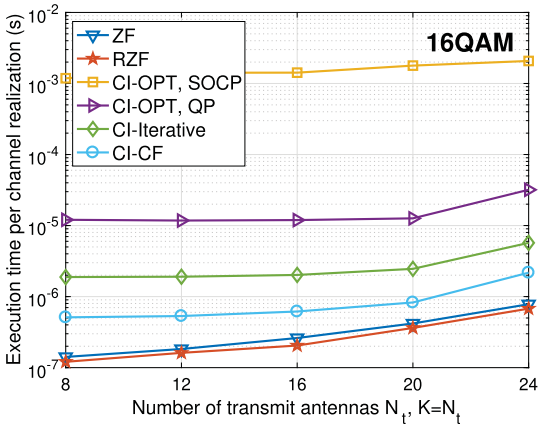

Fig. 8. Execution time v.s. N_t, 16QAM, $K = N_t$.

achieves an improved performance over ZF precoding for all SNRs, while also outperforming RZF precoding at high SNR. For high SNRs, we observe a SNR gain of more than 6dB over ZF and 4dB over RZF. Moreover, it is shown that the CI precoding based on the iterative algorithm 'CI-Iterative' achieves exactly the same performance as the optimization-based CI precoding 'CI-OPT', which validates its optimality in obtaining the precoding matrix. While the sub-optimal closed-form precoder 'CI-CF' is inferior to optimal CI precoding, we observe that it also outperforms both ZF precoding and RZF precoding when the SNR is high.

In Fig. 6, we compare the BER of different precoding approaches for 16QAM when $K = N_t = 12$, and a similar BER trend compared to the case of $K = N_t = 8$ in Fig. 5 is observed. The optimal CI precoding scheme achieves the best performance and significantly outperform other precoding methods in the high SNR regime, where the SNR gain is as large as 7dB. Compared with Fig. 5, we observe that the performance gains of CI precoding over traditional ZF-based precoding schemes are more significant when the number of users and antennas increases.

We further consider a higher-order 64QAM modulation and present the corresponding BER result in Fig. 7. Similar to the case of 16QAM, both the optimal CI precoding and the sub-optimal closed-form CI precoding methods achieve an improved performance over ZF precoding. More importantly, in contrast to claims that CI precoding may not be promising for higher-order QAM modulations where only the outer constellation points can exploit CI, we show that the performance gains of CI precoding over ZF can be as large as 5dB, since CI precoding not only relaxes the optimization area for the outer constellation points, where the total number of constellation points that are optimized for a $\mathcal{M}$-QAM constellation is $\left(8\sqrt{\frac{\mathcal{M}}{4}} - 4\right)$ ($\frac{28}{64} = 43.75\%$ for 64-QAM), but also reduces the noise amplification effect for the precoder. Both of the above contribute to the performance improvements over ZF precoding.

In Fig. 8, we evaluate the computational cost of each precoding scheme in terms of the execution time per channel realization, as an indication to show the potential complexity benefits of the proposed iterative closed-form CI solution, where 'CI-OPT, SOCP' refers to the optimization problem $\mathcal{P}_3$, 'CI-OPT, QP' refers to $\mathcal{P}_5$ and 'CI-OPT, Iterative' refers to Algorithm 1. We observe that solving the equivalent QP problem is much more efficient than solving the original SOCP problem. More importantly, our proposed iterative algorithm exhibits additional complexity gain than the QP method, which further motivates the use of CI precoding in practical communication systems.

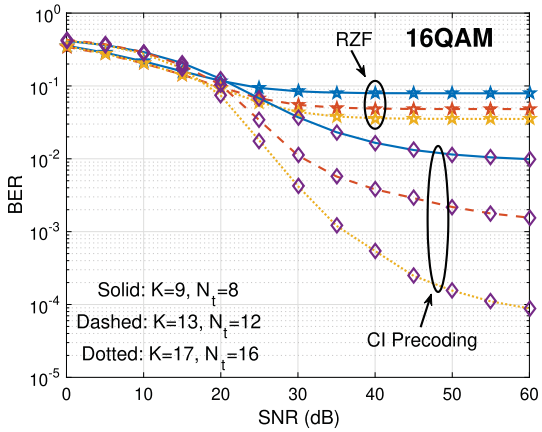

Fig. 9. Uncoded BER v.s. SNR, 16QAM, $K > N_t$.

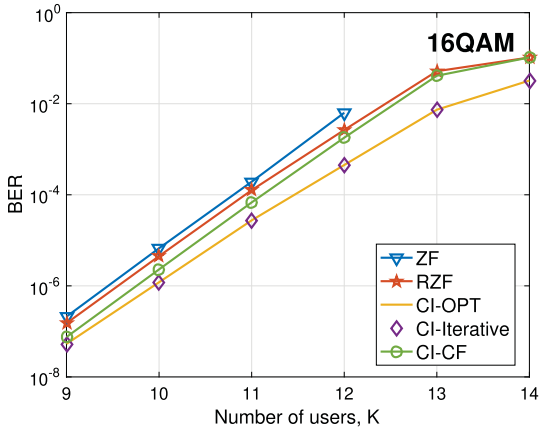

Fig. 10. Uncoded BER v.s. number of users K, 16QAM, $N_t = 12$, SNR=35dB.

B. $K > N_t$

In this section, we consider the scenario of $K > N_t$. Fig. 9 depicts the BER result of 3 antenna settings for 16QAM modulation. ZF precoding is not applicable in these cases, and therefore we compare with RZF precoding. When CI precoding does not return a valid solution, as discussed in Section IV-A, RZF precoding is employed instead. For all of the three considered scenarios, we observe that at high SNRs the average BER performance for CI precoding achieves a significant performance gain over traditional RZF precoding, since there is a high probability of a feasible solution for CI precoding when $K - N_t = 1$, as illustrated later in Fig. 11. Moreover, we observe that the performance gains further increase with an increase in the number of transmit antennas.

We present the BER result with respect to an increasing number of users in Fig. 10 for 16QAM, where $N_t = 12$ and SNR=35dB. ZF precoding does not apply for the case of $K > N_t$ and therefore does not have a BER result when $K > 12$. For both the case of $K \leq N_t$ and $K > N_t$, we observe that CI precoding achieves the best BER performance, and the performance gains over ZF-based precoding are more significant when K increases, which is due to the fact that the optimal CI precoding is more likely to be ZF precoding when K is small.

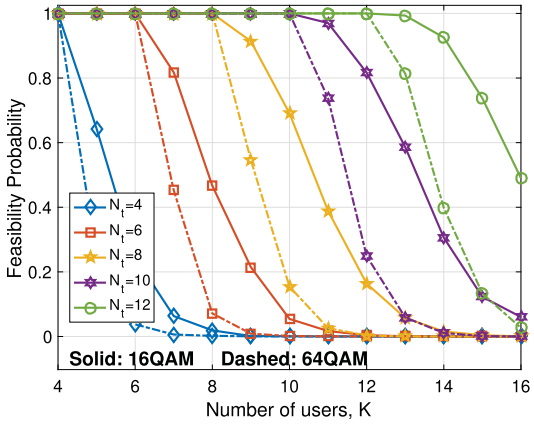

Fig. 11. Feasibility probability v.s. number of users K.

In Fig. 11, we present the average feasibility probability for the case of $K > N_t$ with an increasing number of users, where the performance of 16QAM and 64QAM modulations are denoted as solid and dashed lines, respectively. Generally, we observe that a larger number of antennas at the BS leads to a higher probability of supporting more users than the number of antennas at the BS. For example, for 16QAM modulation, the BS can support 3 more users when $N_t = 12$ with more than a 70% feasibility probability, compared to the $N_t = 6$ case where the BS can only support at most only 1 additional user with the same feasibility probability. Specifically, we observe that the feasibility probability for the case of $K = 13$ and $N_t = 12$ is very close to 100% for 16QAM. A similar trend is also observed for 64QAM modulation, although the supported number of users is smaller compared to 16QAM for the same feasibility probability.

VII. Conclusion

In this paper, interference-exploitation precoding for multi-level modulations is studied. By analyzing the optimization problems and their corresponding Lagrangian and KKT conditions, we mathematically show that interference-exploitation precoding is equivalent to a QP optimization, based on which we derive the optimal precoding matrix as a function of the variables for the QP optimization as well as a sub-optimal closed-form precoder. Numerical results show that the optimal precoding matrix can be efficiently obtained by the proposed iterative algorithm, and the superior performance improvement of interference-exploitation precoding over traditional precoding schemes is also observed for multi-level modulations.

Appendix A
Proof for Lemma 1

We first prove the equivalency between $\mathcal{P}_1$ and $\mathcal{P}_2$ for a generic $\mathcal{M}$-PSK modulation. To begin with, we first give a generic expression of each data symbol $s_{(l)}$ for a generic $\mathcal{M}$-PSK modulation based on Fig. 12 depicted below [29]:

$$s_{(l)} = e^{j\cdot\left[\frac{2\pi}{\mathcal{M}}(l-1)+\frac{\pi}{4}\right]},\ \forall l \in \{1, 2, \cdots, \mathcal{M}\}. \qquad (51)$$

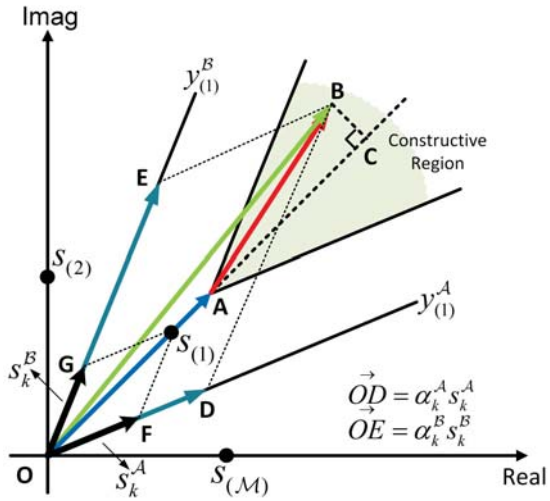

Fig. 12. Constellation of a generic $\mathcal{M}$-PSK modulation.

Based on our decomposition $s_k = s_{(l)} = s^{\mathcal{A}}_k + s^{\mathcal{B}}_k$, we have

$$s^{\mathcal{A}}_k = \frac{e^{j\cdot\left(\frac{2\pi}{\mathcal{M}}\cdot l+\frac{\pi}{4}-\frac{3\pi}{\mathcal{M}}\right)}}{\rho} = \frac{1}{\rho}\left(A^{\Re}_k + j\cdot A^{\Im}_k\right),$$
$$s^{\mathcal{B}}_k = \frac{e^{j\cdot\left(\frac{2\pi}{\mathcal{M}}\cdot l+\frac{\pi}{4}-\frac{\pi}{\mathcal{M}}\right)}}{\rho} = \frac{1}{\rho}\left(B^{\Re}_k + j\cdot B^{\Im}_k\right), \quad (52)$$

where $\rho = \left|e^{j\cdot\left(\frac{2\pi}{\mathcal{M}}\cdot l+\frac{\pi}{4}-\frac{3\pi}{\mathcal{M}}\right)} + e^{j\cdot\left(\frac{2\pi}{\mathcal{M}}\cdot l+\frac{\pi}{4}-\frac{\pi}{\mathcal{M}}\right)}\right|$ is the normalization factor to guarantee that $|s_k| = 1$, and we obtain

$$A^{\Re}_k = \cos\left(\frac{2\pi}{\mathcal{M}}\cdot l+\frac{\pi}{4}-\frac{3\pi}{\mathcal{M}}\right),$$
$$A^{\Im}_k = \sin\left(\frac{2\pi}{\mathcal{M}}\cdot l+\frac{\pi}{4}-\frac{3\pi}{\mathcal{M}}\right),$$
$$B^{\Re}_k = \cos\left(\frac{2\pi}{\mathcal{M}}\cdot l+\frac{\pi}{4}-\frac{\pi}{\mathcal{M}}\right),$$
$$B^{\Im}_k = \sin\left(\frac{2\pi}{\mathcal{M}}\cdot l+\frac{\pi}{4}-\frac{\pi}{\mathcal{M}}\right). \quad (53)$$

Given that $\vec{OB} = \lambda_k s_k = \alpha^{\mathcal{A}}_k s^{\mathcal{A}}_k + \alpha^{\mathcal{B}}_k s^{\mathcal{B}}_k$ and by following the coordinate transformation in [29], $\alpha^{\mathcal{A}}_k$ and $\alpha^{\mathcal{B}}_k$ can be expressed as a function of λ_k:

$$\alpha^{\mathcal{A}}_k = \rho\frac{B^{\Im}_k s^{\Re}_k - B^{\Re}_k s^{\Im}_k}{A^{\Re}_k B^{\Im}_k - A^{\Im}_k B^{\Re}_k}\cdot\lambda^{\Re}_k - \rho\frac{B^{\Im}_k s^{\Im}_k + B^{\Re}_k s^{\Re}_k}{A^{\Re}_k B^{\Im}_k - A^{\Im}_k B^{\Re}_k}\cdot\lambda^{\Im}_k,$$
$$\alpha^{\mathcal{B}}_k = \rho\frac{A^{\Re}_k s^{\Im}_k - A^{\Im}_k s^{\Re}_k}{A^{\Re}_k B^{\Im}_k - A^{\Im}_k B^{\Re}_k}\cdot\lambda^{\Re}_k + \rho\frac{A^{\Re}_k s^{\Re}_k + A^{\Im}_k s^{\Im}_k}{A^{\Re}_k B^{\Im}_k - A^{\Im}_k B^{\Re}_k}\cdot\lambda^{\Im}_k. \quad (54)$$

Subsequently, based on the fact that an identical scaling on both $\alpha^{\mathcal{A}}_k$ and $\alpha^{\mathcal{B}}_k$ does not affect the max-min solution, $\max\min\left\{\alpha^{\mathcal{A}}_k, \alpha^{\mathcal{B}}_k\right\}$ is equivalent to $\max\min\left\{\tilde{\alpha}^{\mathcal{A}}_k, \tilde{\alpha}^{\mathcal{B}}_k\right\}$, where

$$\begin{aligned}\tilde{\alpha}^{\mathcal{A}}_k &= \frac{1}{\rho}\left(A^{\Re}_k B^{\Im}_k - A^{\Im}_k B^{\Re}_k\right)\cdot\alpha^{\mathcal{A}}_k \\ &= \left(B^{\Im}_k s^{\Re}_k - B^{\Re}_k s^{\Im}_k\right)\cdot\lambda^{\Re}_k - \left(B^{\Im}_k s^{\Im}_k + B^{\Re}_k s^{\Re}_k\right)\cdot\lambda^{\Im}_k, \\ \tilde{\alpha}^{\mathcal{B}}_k &= \frac{1}{\rho}\left(A^{\Re}_k B^{\Im}_k - A^{\Im}_k B^{\Re}_k\right)\cdot\alpha^{\mathcal{B}}_k \\ &= \left(A^{\Re}_k s^{\Im}_k - A^{\Im}_k s^{\Re}_k\right)\cdot\lambda^{\Re}_k + \left(A^{\Re}_k s^{\Re}_k + A^{\Im}_k s^{\Im}_k\right)\cdot\lambda^{\Im}_k. \end{aligned} \quad (55)$$

Given that $s^{\Re}_k = \cos\left[\frac{2\pi}{\mathcal{M}}(l-1)+\frac{\pi}{4}\right]$, $s^{\Im}_k = \sin\left[\frac{2\pi}{\mathcal{M}}(l-1)+\frac{\pi}{4}\right]$ and by substituting the expressions for $A^{\Re}_k$, $A^{\Im}_k$, $B^{\Re}_k$ and $B^{\Im}_k$ into (55), the expressions for $\tilde{\alpha}^{\mathcal{A}}_k$ and $\tilde{\alpha}^{\mathcal{B}}_k$ can be further simplified, as shown in (56), on the bottom of this page, which is derived based on the sum/difference trigonometric identities. By taking into account the fact that $\lambda^{\Im}_k$ can be negative, we obtain that $\max\min\left\{\alpha^{\mathcal{A}}_k, \alpha^{\mathcal{A}}_k\right\}$ is equivalent to

$$\max\left\{\sin\left(\frac{\pi}{\mathcal{M}}\right)\cdot\lambda^{\Re}_k - \cos\left(\frac{\pi}{\mathcal{M}}\right)\cdot\left|\lambda^{\Im}_k\right|\right\}. \quad (57)$$

By further performing a rescaling by $\sin\left(\frac{\pi}{\mathcal{M}}\right)$, we can obtain that $\max\min\left\{\alpha^{\mathcal{A}}_k, \alpha^{\mathcal{B}}_k\right\}$ is finally equivalent to $\max\left(\lambda^{\Re}_k - \frac{\left|\lambda^{\Im}_k\right|}{\tan\left(\frac{\pi}{\mathcal{M}}\right)}\right)$. Subsequently, by constructing an auxiliary variable t_k as

$$t_k = \lambda^{\Re}_k - \frac{\left|\lambda^{\Im}_k\right|}{\tan\left(\frac{\pi}{\mathcal{M}}\right)}, \quad (58)$$

$$\begin{aligned}\tilde{\alpha}^{\mathcal{A}}_k &= \left\{\cos\left[\frac{2\pi}{\mathcal{M}}(l-1)+\frac{\pi}{4}\right]\sin\left(\frac{2\pi}{\mathcal{M}}\cdot l+\frac{\pi}{4}-\frac{\pi}{\mathcal{M}}\right) - \sin\left[\frac{2\pi}{\mathcal{M}}(l-1)+\frac{\pi}{4}\right]\cos\left(\frac{2\pi}{\mathcal{M}}\cdot l+\frac{\pi}{4}-\frac{\pi}{\mathcal{M}}\right)\right\}\cdot\lambda^{\Re}_k \\ &\quad - \left\{\sin\left(\frac{2\pi}{\mathcal{M}}\cdot l+\frac{\pi}{4}-\frac{\pi}{\mathcal{M}}\right)\sin\left[\frac{2\pi}{\mathcal{M}}(l-1)+\frac{\pi}{4}\right] + \cos\left(\frac{2\pi}{\mathcal{M}}\cdot l+\frac{\pi}{4}-\frac{\pi}{\mathcal{M}}\right)\cos\left[\frac{2\pi}{\mathcal{M}}(l-1)+\frac{\pi}{4}\right]\right\}\cdot\lambda^{\Im}_k \\ &= \sin\left[\frac{2\pi}{\mathcal{M}}\cdot l+\frac{\pi}{4}-\frac{\pi}{\mathcal{M}}-\frac{2\pi}{\mathcal{M}}(l-1)-\frac{\pi}{4}\right]\cdot\lambda^{\Re}_k - \cos\left[\frac{2\pi}{\mathcal{M}}\cdot l+\frac{\pi}{4}-\frac{\pi}{\mathcal{M}}-\frac{2\pi}{\mathcal{M}}(l-1)-\frac{\pi}{4}\right]\cdot\lambda^{\Im}_k \\ &= \sin\left(\frac{\pi}{\mathcal{M}}\right)\cdot\lambda^{\Re}_k - \cos\left(\frac{\pi}{\mathcal{M}}\right)\cdot\lambda^{\Im}_k, \\ \tilde{\alpha}^{\mathcal{B}}_k &= \left\{\cos\left(\frac{2\pi}{\mathcal{M}}\cdot l+\frac{\pi}{4}-\frac{3\pi}{\mathcal{M}}\right)\sin\left[\frac{2\pi}{\mathcal{M}}(l-1)+\frac{\pi}{4}\right] - \sin\left(\frac{2\pi}{\mathcal{M}}\cdot l+\frac{\pi}{4}-\frac{3\pi}{M}\right)\cos\left[\frac{2\pi}{\mathcal{M}}(l-1)+\frac{\pi}{4}\right]\right\}\cdot\lambda^{\Re}_k \\ &\quad + \left\{\cos\left(\frac{2\pi}{\mathcal{M}}\cdot l+\frac{\pi}{4}-\frac{3\pi}{\mathcal{M}}\right)\cos\left[\frac{2\pi}{\mathcal{M}}(l-1)+\frac{\pi}{4}\right] + \sin\left(\frac{2\pi}{\mathcal{M}}\cdot l+\frac{\pi}{4}-\frac{3\pi}{\mathcal{M}}\right)\sin\left[\frac{2\pi}{\mathcal{M}}(l-1)+\frac{\pi}{4}\right]\right\}\cdot\lambda^{\Im}_k \\ &= \sin\left[\frac{2\pi}{\mathcal{M}}(l-1)+\frac{\pi}{4}-\frac{2\pi}{\mathcal{M}}\cdot l-\frac{\pi}{4}+\frac{3\pi}{\mathcal{M}}\right]\cdot\lambda^{\Re}_k + \cos\left[\frac{2\pi}{\mathcal{M}}(l-1)+\frac{\pi}{4}-\frac{2\pi}{\mathcal{M}}\cdot l-\frac{\pi}{4}+\frac{3\pi}{\mathcal{M}}\right]\cdot\lambda^{\Im}_k \\ &= \sin\left(\frac{\pi}{\mathcal{M}}\right)\cdot\lambda^{\Re}_k + \cos\left(\frac{\pi}{\mathcal{M}}\right)\cdot\lambda^{\Im}_k. \end{aligned} \quad (56)$$

$\max\min\left\{\alpha_k^{\mathcal{A}}, \alpha_k^{\mathcal{B}}\right\}$ is equivalent to $\max t_k$. Accordingly, $\mathcal{P}_2$ can be equivalently transformed into

$$\begin{aligned}\mathcal{P}_9: \ &\max_{\mathbf{W},\lambda_k}\min_k \ t_k \\ &s.t.\ \mathbf{C1}: \mathbf{h}_k^T\mathbf{W}\mathbf{s} = \lambda_k s_k,\ \forall k \in \mathcal{K} \\ &\quad \mathbf{C2}: t_k = \lambda_k^{\Re} - \frac{\left|\lambda_k^{\Im}\right|}{\tan\left(\frac{\pi}{\mathcal{M}}\right)},\ \forall k \in \mathcal{K} \\ &\quad \mathbf{C3}: \|\mathbf{W}\mathbf{s}\|_2^2 \le p_0 \end{aligned} \tag{59}$$

By reformulating the above max-min problem $\mathcal{P}_9$ into a max problem, we arrive at $\mathcal{P}_1$, which completes the proof.

The second part of this lemma can be proven by contradiction based on the observation that the objective function t for $\mathcal{P}_1$ can be further increased if none of the noiseless received signals are located on the boundary. Subsequently, (9) is derived by considering the isosceles triangle 'DOA' in Fig. 1c, where based on the Pythagorean theorem we can obtain

$$|\vec{OA}| = 2|\vec{DO}|\cos\angle_{DOA}. \tag{60}$$

Based on the fact that $|\vec{OA}| = t^*$, $|\vec{DO}| = |\vec{DA}| = \left(\alpha_k^{\mathcal{U}}\right)^*\left|\left(s_k^{\mathcal{U}}\right)^*\right|$, and $\angle_{DOA} = \frac{\pi}{\mathcal{M}}$, (60) leads to the expression for t^* in (9). ■

APPENDIX B
PROOF FOR PROPOSITION 1

We first transform the power constraint in $\mathcal{P}_3$, where we decompose the precoded signals $\mathbf{W}\mathbf{s}$ into

$$\mathbf{W}\mathbf{s} = \sum_{i=1}^{K}\mathbf{w}_i s_i. \tag{61}$$

Since $\mathbf{W}\mathbf{s}$ can be viewed as a single vector for both constraints that include $\mathbf{W}$ in $\mathcal{P}_3$, how the power is distributed among each $\mathbf{w}_i s_i$ will not affect the solution of the above optimization problem. Therefore, without loss of generality, it is safe to assume that each term $\mathbf{w}_i s_i$ is identical, which leads to

$$\|\mathbf{W}\mathbf{s}\|_2^2 = \|K\mathbf{w}_i s_i\|_2^2 = K^2 s_i^*\mathbf{w}_i^H\mathbf{w}_i s_i = K\sum_{i=1}^{K} s_i^*\mathbf{w}_i^H\mathbf{w}_i s_i, \tag{62}$$

and the original power constraint $\|\mathbf{W}\mathbf{s}\|_2^2 \le p_0$ is equivalent to

$$\|\mathbf{W}\mathbf{s}\|_2^2 \le p_0 \Rightarrow \sum_{i=1}^{K} s_i^*\mathbf{w}_i^H\mathbf{w}_i s_i \le \frac{p_0}{K}. \tag{63}$$

We then rewrite the considered optimization problem $\mathcal{P}_3$ in a standard minimization form as

$$\begin{aligned}\mathcal{P}_{10}: \ &\min_{\mathbf{W},\mathbf{\Omega}_k,t} \ -t \\ &s.t.\ \mathbf{C1}: \mathbf{h}_k^T\sum_{i=1}^{K}\mathbf{w}_i s_i - \mathbf{\Omega}_k^T\mathbf{s}_k = 0,\ \forall k \in \mathcal{K} \\ &\quad \mathbf{C2}: t - \alpha_m^{\mathcal{O}} \le 0,\ \forall \alpha_m^{\mathcal{O}} \in \mathcal{O} \\ &\quad \mathbf{C3}: t - \alpha_n^{\mathcal{I}} = 0,\ \forall \alpha_n^{\mathcal{I}} \in \mathcal{I} \\ &\quad \mathbf{C4}: \sum_{i=1}^{K} s_i^*\mathbf{w}_i^H\mathbf{w}_i s_i \le \frac{p_0}{K} \end{aligned} \tag{64}$$

and following [42] we construct the Lagrangian of $\mathcal{P}_{10}$ as

$$\begin{aligned}&\mathcal{L}\left(\mathbf{w}_i, t, \delta_k, \mu_m, \nu_n, \delta_0\right) \\ &= -t \\ &\quad + \sum_{k=1}^{K}\delta_k\left(\mathbf{h}_k^T\sum_{i=1}^{K}\mathbf{w}_i s_i - \mathbf{\Omega}_k^T\mathbf{s}_k\right) + \sum_{m=1}^{card\{\mathcal{O}\}}\mu_m\left(t - \alpha_m^{\mathcal{O}}\right) \\ &\quad + \sum_{n=1}^{card\{\mathcal{I}\}}\nu_n\left(t - \alpha_n^{\mathcal{I}}\right) + \delta_0\left(\sum_{i=1}^{K} s_i^*\mathbf{w}_i^H\mathbf{w}_i s_i - \frac{p_0}{K}\right), \end{aligned} \tag{65}$$

where δ_k, μ_m, ν_n, and δ_0 are the introduced dual variables, $\delta_0 \ge 0$ and $\mu_m \ge 0$, $\forall m \in \{1, 2, \cdots, card\{\mathcal{O}\}\}$. Each δ_k and ν_n can be complex since they correspond to the equality constraints.

Based on the Lagrangian in (65), the KKT conditions for optimality can be expressed as

$$\frac{\partial\mathcal{L}}{\partial t} = -1 + \sum_{m=1}^{card\{\mathcal{O}\}}\mu_m + \sum_{n=1}^{card\{\mathcal{I}\}}\nu_n = 0 \tag{66a}$$

$$\frac{\partial\mathcal{L}}{\partial\mathbf{w}_i} = \left(\sum_{k=1}^{K}\delta_k\cdot\mathbf{h}_k^T\right)s_i + \delta_0 s_i s_i^*\cdot\mathbf{w}_i^H = \mathbf{0},\ \forall i \in \mathcal{K} \tag{66b}$$

$$\mathbf{h}_k^T\sum_{i=1}^{K}\mathbf{w}_i s_i - \mathbf{\Omega}_k^T\mathbf{s}_k = 0,\ \forall k \in \mathcal{K} \tag{66c}$$

$$\mu_m\left(t - \alpha_m^{\mathcal{O}}\right) = 0,\ \forall \alpha_m^{\mathcal{O}} \in \mathcal{O} \tag{66d}$$

$$t - \alpha_n^{\mathcal{I}} = 0,\ \forall \alpha_n^{\mathcal{I}} \in \mathcal{I} \tag{66e}$$

$$\delta_0\left(\sum_{i=1}^{K} s_i^*\mathbf{w}_i^H\mathbf{w}_i s_i - \frac{p_0}{K}\right) = 0 \tag{66f}$$

Based on (66b), it is first observed that $\delta_0 \ne 0$, and with the premise that $\delta_0 \ge 0$ we obtain $\delta_0 > 0$, which further means that the power constraint is met with equality when optimality is achieved. Then, we can express $\mathbf{w}_i^H$ in (66b) as

$$\mathbf{w}_i^H = -\frac{s_i}{\delta_0 s_i s_i^*}\left(\sum_{k=1}^{K}\delta_k\cdot\mathbf{h}_k^T\right) = -\frac{1}{s_i^*}\left(\sum_{k=1}^{K}\frac{\delta_k}{\delta_0}\cdot\mathbf{h}_k^T\right). \tag{67}$$

By introducing an auxiliary variable

$$\vartheta_k = -\frac{\delta_k^H}{\delta_0},\ \forall k \in \mathcal{K}, \tag{68}$$

we can express $\mathbf{w}_i$ as

$$\mathbf{w}_i = \left(\sum_{k=1}^{K}\vartheta_k\cdot\mathbf{h}_k^*\right)\frac{1}{s_i},\ \forall i \in \mathcal{K}. \tag{69}$$

The above expression further leads to

$$\mathbf{w}_i s_i = \left(\sum_{k=1}^{K}\vartheta_k\cdot\mathbf{h}_k^*\right),\ \forall i \in \mathcal{K}, \tag{70}$$

which is constant for any i and consistent with our assumption in (62).

With the obtained expression for each $\mathbf{w}_i$, we further express the precoding matrix $\mathbf{W}$ as

$$\begin{aligned}\mathbf{W} &= [\mathbf{w}_1, \mathbf{w}_2, \cdots, \mathbf{w}_K] \\ &= \left(\sum_{k=1}^{K} \vartheta_k \cdot \mathbf{h}_k^*\right) \left[\frac{1}{s_1}, \frac{1}{s_2}, \cdots, \frac{1}{s_K}\right] \\ &= [\mathbf{h}_1^*, \mathbf{h}_2^*, \cdots, \mathbf{h}_K^*] [\vartheta_1, \vartheta_2, \cdots, \vartheta_K]^T \left[\frac{1}{s_1}, \frac{1}{s_2}, \cdots, \frac{1}{s_K}\right] \\ &= \mathbf{H}^H \boldsymbol{\Upsilon} \hat{\mathbf{s}}^T, \end{aligned} \tag{71}$$

where we have introduced two column vectors

$$\boldsymbol{\Upsilon} = [\vartheta_1, \vartheta_2, \cdots, \vartheta_K]^T, \ \hat{\mathbf{s}} = \left[\frac{1}{s_1}, \frac{1}{s_2}, \cdots, \frac{1}{s_K}\right]^T. \tag{72}$$

We further express (10) in a matrix form as

$$\begin{aligned}\mathbf{HWs} &= \left[\boldsymbol{\Omega}_1^T \mathbf{s}_1, \boldsymbol{\Omega}_2^T \mathbf{s}_2, \cdots, \boldsymbol{\Omega}_K^T \mathbf{s}_K\right]^T \\ &= \mathbf{U} diag\left(\boldsymbol{\Omega}\right) \mathbf{s_E}, \end{aligned} \tag{73}$$

where $\boldsymbol{\Omega} \in \mathcal{R}^{2K\times 1}$ and $\mathbf{s_E} \in \mathcal{R}^{2K\times 1}$ are expressed as

$$\begin{aligned}\boldsymbol{\Omega} &= \left[\boldsymbol{\Omega}_1^T, \boldsymbol{\Omega}_2^T, \cdots, \boldsymbol{\Omega}_K^T\right]^T \\ &= \left[\alpha_1^{\mathcal{A}}, \alpha_1^{\mathcal{B}}, \alpha_2^{\mathcal{A}}, \alpha_2^{\mathcal{B}}, \cdots, \alpha_K^{\mathcal{A}}, \alpha_K^{\mathcal{B}}\right]^T \\ &= \left[\alpha_1^E, \alpha_2^E, \cdots, \alpha_{2K-1}^E, \alpha_{2K}^E\right]^T, \\ \mathbf{s_E} &= \left[\mathbf{s}_1^T, \mathbf{s}_2^T, \cdots, \mathbf{s}_K^T\right]^T \\ &= \left[s_1^{\mathcal{A}}, s_1^{\mathcal{B}}, s_2^{\mathcal{A}}, s_2^{\mathcal{B}}, \cdots, s_K^{\mathcal{A}}, s_K^{\mathcal{B}}\right]^T \\ &= \left[s_1^E, s_2^E, \cdots, s_{2K-1}^E, s_{2K}^E\right]^T, \end{aligned} \tag{74}$$

and the matrix $\mathbf{U} \in \mathcal{C}^{K\times 2K}$ is constructed as

$$\mathbf{U} = \begin{bmatrix} 1 & 1 & 0 & 0 & \cdots & 0 & 0 \\ 0 & 0 & 1 & 1 & \ddots & \vdots & \vdots \\ \vdots & \vdots & \ddots & \ddots & \ddots & \vdots & \vdots \\ \vdots & \vdots & \ddots & \ddots & \ddots & 0 & 0 \\ 0 & 0 & \cdots & 0 & 0 & 1 & 1 \end{bmatrix} = \mathbf{I}_K \otimes [1, 1]. \tag{75}$$

By substituting the expression for $\mathbf{W}$ in (71) into (73), we obtain

$$\mathbf{H}\mathbf{H}^H \boldsymbol{\Upsilon} \hat{\mathbf{s}}^T \mathbf{s} = \mathbf{U} diag\left(\boldsymbol{\Omega}\right) \mathbf{s_E}. \tag{76}$$

With the premise that $K \leq N_t$ in Section III, $\mathbf{H}\mathbf{H}^H$ is invertible, and accordingly we obtain $\boldsymbol{\Upsilon}$ as

$$\boldsymbol{\Upsilon} = \frac{1}{K} \cdot \left(\mathbf{H}\mathbf{H}^H\right)^{-1} \mathbf{U} diag\left(\boldsymbol{\Omega}\right) \mathbf{s_E}. \tag{77}$$

By substituting the expression for $\boldsymbol{\Upsilon}$ into $\mathbf{W}$ in (71), (15) is obtained, which completes the proof. ■

APPENDIX C
PROOF FOR PROPOSITION 2

The Lagrangian of $\mathcal{P}_4$ is formulated as

$$\begin{aligned}&\mathcal{L}\left(\boldsymbol{\Omega}, t, \delta_0, \mu_m, \nu_n\right) \\ &\quad = -t + \delta_0 \left(\boldsymbol{\Omega}^T \mathbf{V} \boldsymbol{\Omega} - p_0\right) \\ &\qquad + \sum_{m=1}^{card\{\mathcal{O}\}} \mu_m \left(t - \alpha_m^{\mathcal{O}}\right) + \sum_{n=1}^{card\{\mathcal{I}\}} \nu_n \left(t - \alpha_n^{\mathcal{I}}\right), \end{aligned} \tag{78}$$

where $\mu_m \geq 0$, $\forall m \in \{1, 2, \cdots, card\{\mathcal{O}\}\}$. To simplify the subsequent KKT conditions, we propose to rearrange the columns and rows of the matrices and vectors included in the Lagrangian expression in (78). Specifically, we rearrange the expanded symbol vector $\mathbf{s_E}$ into

$$\mathbf{s_E} \Rightarrow \tilde{\mathbf{s}}_{\mathbf{E}} = \left[\tilde{\mathbf{s}}_{\mathcal{O}}^T, \tilde{\mathbf{s}}_{\mathcal{I}}^T\right]^T, \tag{79}$$

where $\tilde{\mathbf{s}}_{\mathcal{O}} \in \mathcal{R}^{card\{\mathcal{O}\}\times 1}$ and $\tilde{\mathbf{s}}_{\mathcal{I}} \in \mathcal{R}^{card\{\mathcal{I}\}\times 1}$ are given by

$$\begin{aligned}\tilde{\mathbf{s}}_{\mathcal{O}} &= \left[\tilde{s}_1, \tilde{s}_2, \cdots, \tilde{s}_{card\{\mathcal{O}\}}\right]^T, \\ \tilde{\mathbf{s}}_{\mathcal{I}} &= \left[\tilde{s}_{card\{\mathcal{O}\}+1}, \tilde{s}_{card\{\mathcal{O}\}+2}, \cdots, \tilde{s}_{2K}\right]^T, \end{aligned} \tag{80}$$

such that the entries in $\tilde{\mathbf{s}}_{\mathcal{O}}$ correspond to the real or imaginary part of the outer constellation points that can exploit CI, and the entries in $\tilde{\mathbf{s}}_{\mathcal{I}}$ correspond to the real and imaginary part of the inner constellation points that cannot be scaled. The corresponding scaling vector $\boldsymbol{\Omega}$ is accordingly transformed into

$$\boldsymbol{\Omega} \Rightarrow \tilde{\boldsymbol{\Omega}} = \left[\tilde{\boldsymbol{\Omega}}_{\mathcal{O}}^T, \tilde{\boldsymbol{\Omega}}_{\mathcal{I}}^T\right]^T, \tag{81}$$

where $\tilde{\boldsymbol{\Omega}}_{\mathcal{O}} \in \mathcal{R}^{card\{\mathcal{O}\}\times 1}$ and $\tilde{\boldsymbol{\Omega}}_{\mathcal{I}} \in \mathcal{R}^{card\{\mathcal{I}\}\times 1}$ are given by

$$\begin{aligned}\tilde{\boldsymbol{\Omega}}_{\mathcal{O}} &= \left[\tilde{\alpha}_1, \tilde{\alpha}_2, \cdots, \tilde{\alpha}_{card\{\mathcal{O}\}}\right]^T, \\ \tilde{\boldsymbol{\Omega}}_{\mathcal{I}} &= \left[\tilde{\alpha}_{card\{\mathcal{O}\}+1}, \tilde{\alpha}_{card\{\mathcal{O}\}+2}, \cdots, \tilde{\alpha}_{2K}\right]^T. \end{aligned} \tag{82}$$

We further introduce a '**Locater**' function that returns the index of $\tilde{s}_m$ in the original expanded symbol vector $\mathbf{s_E}$, given by

$$\mathrm{L}\left(\tilde{s}_m\right) = k, \text{ if } \tilde{s}_m = s_k^E. \tag{83}$$

We can then express $\tilde{\mathbf{s}}_{\mathbf{E}}$ and $\tilde{\boldsymbol{\Omega}}$ as

$$\tilde{\mathbf{s}}_{\mathbf{E}} = \mathbf{F}\mathbf{s_E}, \ \tilde{\boldsymbol{\Omega}} = \mathbf{F}\boldsymbol{\Omega}, \tag{84}$$

where the transformation matrix $\mathbf{F} \in \mathcal{R}^{2K\times 2K}$ that transforms the original $\boldsymbol{\Omega}$ and $\mathbf{s_E}$ into their rearranged forms is given by

$$\mathbf{F} = \left[\mathbf{e}_{\mathrm{L}(\tilde{s}_1)}, \mathbf{e}_{\mathrm{L}(\tilde{s}_2)}, \cdots, \mathbf{e}_{\mathrm{L}(\tilde{s}_{2K})}\right]^T, \tag{85}$$

and we note that $\mathbf{F}$ is invertible. Similarly, the corresponding rearranged matrix $\tilde{\mathbf{V}}$ can be obtained as

$$\tilde{\mathbf{V}} = \mathbf{F}\mathbf{V}\mathbf{F}^T, \tag{86}$$

where the multiplication of $\mathbf{F}$ at the left side and $\mathbf{F}^T$ at the right side correspond to the row and column rearrangement, respectively. Using the above expressions for $\tilde{\mathbf{s}}$, $\tilde{\boldsymbol{\Omega}}$ and $\tilde{\mathbf{V}}$, the Lagrangian of $\mathcal{P}_4$ in (78) can be further transformed into a simple form, given by

$$\mathcal{L}\left(\tilde{\boldsymbol{\Omega}}, t, \delta_0, \mathbf{u_1}\right) = \left(\mathbf{1}^T \mathbf{u_1} - 1\right) t + \delta_0 \cdot \tilde{\boldsymbol{\Omega}}^T \tilde{\mathbf{V}} \tilde{\boldsymbol{\Omega}} - \mathbf{u_1}^T \tilde{\boldsymbol{\Omega}} - \delta_0 p_0, \tag{87}$$

where $\mathbf{1} = [1, 1, \cdots, 1]^T \in \mathcal{R}^{2K\times 1}$, and $\mathbf{u_1} \in \mathcal{R}^{2K\times 1}$ is the dual vector corresponding to the rearranged $\tilde{\boldsymbol{\Omega}}$, given by

$$\mathbf{u_1} = \left[\mu_1, \mu_2, \cdots, \mu_{card\{\mathcal{O}\}}, \nu_1, \nu_2, \cdots, \nu_{card\{\mathcal{I}\}}\right]^T. \tag{88}$$

Subsequently, the KKT conditions for $\mathcal{P}_5$ can be formulated as

$$\frac{\partial \mathcal{L}}{\partial t} = \mathbf{1}^T \mathbf{u_1} - 1 = 0 \tag{89a}$$

$$\frac{\partial \mathcal{L}}{\partial \tilde{\mathbf{\Omega}}} = \delta_0 \cdot 2\tilde{\mathbf{V}}\tilde{\mathbf{\Omega}} - \mathbf{u_1} = \mathbf{0} \tag{89b}$$

$$\tilde{\mathbf{\Omega}}^T\tilde{\mathbf{V}}\tilde{\mathbf{\Omega}} - p_0 = 0 \tag{89c}$$

$$\mu_m\left(t - \tilde{\alpha}_m\right) = 0,\ \forall m \in \{1, 2, \cdots, card\{\mathcal{O}\}\} \tag{89d}$$

$$t - \tilde{\alpha}_n = 0,\ \forall n \in \{card\{\mathcal{I}\} + 1, \cdots, 2K\} \tag{89e}$$

Based on (89b), we obtain an expression for $\tilde{\mathbf{\Omega}}$ as a function of $\mathbf{u_1}$, given by

$$\tilde{\mathbf{\Omega}} = \frac{1}{2\delta_0} \cdot \tilde{\mathbf{V}}^{-1}\mathbf{u_1}, \tag{90}$$

where we note that $\tilde{\mathbf{V}}$ is symmetric and invertible. By substituting the expression for $\tilde{\mathbf{\Omega}}$ in (90) into the power constraint, we further obtain δ_0 as

$$\begin{aligned}
&\left(\frac{1}{2\delta_0} \cdot \tilde{\mathbf{V}}^{-1}\mathbf{u_1}\right)^T \tilde{\mathbf{V}} \left(\frac{1}{2\delta_0} \cdot \tilde{\mathbf{V}}^{-1}\mathbf{u_1}\right) = p_0 \\
&\Rightarrow\ \frac{1}{4\delta_0^2} \cdot \mathbf{u_1}^T\tilde{\mathbf{V}}^{-1}\tilde{\mathbf{V}}\tilde{\mathbf{V}}^{-1}\mathbf{u_1} = p_0 \\
&\Rightarrow\ \delta_0 = \sqrt{\frac{\mathbf{u_1}^T\tilde{\mathbf{V}}^{-1}\mathbf{u_1}}{4p_0}}.
\end{aligned} \tag{91}$$

For the convex optimization $\mathcal{P}_4$, it is easy to verify that Slater's condition is met [42], which means that the duality gap is zero. Accordingly, $\mathcal{P}_4$ can also be optimally solved via its dual problem, given by

$$\mathcal{P}_{11}:\ \mathcal{D} = \max_{\mathbf{u_1}, \delta_0} \min_{\tilde{\mathbf{\Omega}}, t} \mathcal{L}\left(\mathbf{u_1}, \delta_0, \tilde{\mathbf{\Omega}}, t\right). \tag{92}$$

For the above dual problem, the inner minimization is achieved by (89a) and (90), and we can further simplify the dual problem into

$$\begin{aligned}
\mathcal{D} &= \max_{\mathbf{u_1}, \delta_0}\ \delta_0 \cdot \tilde{\mathbf{\Omega}}^T\tilde{\mathbf{V}}\tilde{\mathbf{\Omega}} + \mathbf{u_1}^T\tilde{\mathbf{\Omega}} - \delta_0 p_0 \\
&= \max_{\mathbf{u_1}, \delta_0}\ \frac{\delta_0}{4\delta_0^2} \cdot \mathbf{u_1}^T\tilde{\mathbf{V}}^{-1}\mathbf{u_1} - \frac{1}{2\delta_0}\mathbf{u_1}^T\tilde{\mathbf{V}}^{-1}\mathbf{u_1} - \delta_0 p_0 \\
&= \max_{\mathbf{u_1}}\ -\frac{\mathbf{u_1}^T\tilde{\mathbf{V}}^{-1}\mathbf{u_1}}{4\sqrt{\frac{\mathbf{u_1}^T\tilde{\mathbf{V}}^{-1}\mathbf{u_1}}{4p_0}}} - \sqrt{\frac{\mathbf{u_1}^T\tilde{\mathbf{V}}^{-1}\mathbf{u_1}}{4p_0}} \cdot p_0 \\
&= \max_{\mathbf{u_1}}\ -\sqrt{p_0 \cdot \mathbf{u_1}^T\tilde{\mathbf{V}}^{-1}\mathbf{u_1}}
\end{aligned} \tag{93}$$

Based on the fact that $y = \sqrt{x}$ is a monotonic function, the above dual problem is equivalent to (21), which completes the proof. ■

APPENDIX D
PROOF FOR LEMMA 2

We first consider the matrix $\mathbf{A} = \mathbf{H}\mathbf{H}^H\left(\mathbf{H}\mathbf{H}^H\right)^+$, and we note that $\mathrm{rank}\{\mathbf{A}\} = N_t$ with probability 1. Accordingly, we can express the eigenvalue decomposition of $\mathbf{A}$ as

$$\mathbf{A} = \mathbf{Q}\mathbf{\Lambda_A}\mathbf{Q}^H, \tag{94}$$

where $\mathbf{Q}$ is a unitary matrix. Based on the construction of the pseudo-inverse [41], $\mathbf{\Lambda_A}$ is given by

$$\mathbf{\Lambda_A} = diag\left\{[1, \cdots, 1, 0, \cdots, 0]^T\right\}, \tag{95}$$

with all the N_t non-zero eigenvalues equal to 1. By further expressing the identity matrix $\mathbf{I}_K$ as

$$\mathbf{I}_K = \mathbf{Q}\mathbf{I}_K\mathbf{Q}^H, \tag{96}$$

we define

$$\begin{aligned}
\mathbf{B} &= \mathbf{H}\mathbf{H}^H\left(\mathbf{H}\mathbf{H}^H\right)^+ - \mathbf{I}_K \\
&= \mathbf{A} - \mathbf{I}_K \\
&= \mathbf{Q}\left(\mathbf{\Lambda_A} - \mathbf{I}_K\right)\mathbf{Q}^H \\
&= \mathbf{Q}\mathbf{\Lambda_B}\mathbf{Q}^H,
\end{aligned} \tag{97}$$

where the last step represents the eigenvalue decomposition of $\mathbf{B}$. Since $\mathbf{\Lambda_B}$ contains $(K - N_t)$ non-zero entries on the diagonal, we obtain that $\mathrm{rank}\{\mathbf{B}\} = K - N_t$. Subsequently, based on the observation that both $\mathbf{U}$ and $diag\left(\mathbf{s_E}\right)$ are full-rank, we therefore have

$$\mathrm{rank}\{\mathbf{P}\} = \mathrm{rank}\{\mathbf{B}\} = K - N_t, \tag{98}$$

which completes the proof. ■

APPENDIX E
PROOF FOR PROPOSITION 3

Based on the obtained expression for $\mathbf{\Omega}$ as a function of $\boldsymbol{\beta}$ in (29), we can now formulate an equivalent optimization on $\boldsymbol{\beta}$, given by

$$\begin{aligned}
\mathcal{P}_{12}:\ &\min_{\boldsymbol{\beta}, t}\ -t \\
&s.t.\ \mathbf{C1}: \boldsymbol{\beta}^T\mathbf{Y}\boldsymbol{\beta} - p_0 = 0 \\
&\quad\ \mathbf{C2}: t - \mathbf{d}_m^T\boldsymbol{\beta} \le 0,\ \forall \alpha_m^{\mathcal{O}} \in \mathcal{O} \\
&\quad\ \mathbf{C3}: t - \mathbf{d}_n^T\boldsymbol{\beta} = 0,\ \forall \alpha_n^{\mathcal{I}} \in \mathcal{I}
\end{aligned} \tag{99}$$

where $\mathbf{Y} = \Re\left(\mathbf{X}\right)$. The Lagrangian of $\mathcal{P}_{12}$ can be expressed as

$$\begin{aligned}
&\mathcal{L}\left(\boldsymbol{\beta}, t, \tilde{\delta}_0, \tilde{\mu}_m, \tilde{\nu}_n\right) \\
&= -t + \tilde{\delta}_0\left(\boldsymbol{\beta}^T\mathbf{Y}\boldsymbol{\beta} - p_0\right) \\
&\quad + \sum_{m=1}^{card\{\mathcal{O}\}} \tilde{\mu}_m\left(t - \mathbf{d}_m^T\boldsymbol{\beta}\right) + \sum_{n=1}^{card\{\mathcal{I}\}} \tilde{\nu}_n\left(t - \mathbf{d}_n^T\boldsymbol{\beta}\right) \\
&= \left(\mathbf{1}^T\mathbf{u_2} - 1\right)t + \tilde{\delta}_0 \cdot \boldsymbol{\beta}^T\mathbf{Y}\boldsymbol{\beta} - \mathbf{u_2}^T\mathbf{F}\mathbf{D}\boldsymbol{\beta} - \tilde{\delta}_0 p_0,
\end{aligned} \tag{100}$$

where the dual vector $\mathbf{u_2}$ for $\mathcal{P}_{12}$ is given by

$$\mathbf{u_2} = \left[\tilde{\mu}_1, \tilde{\mu}_2, \cdots, \tilde{\mu}_{card\{\mathcal{O}\}}, \tilde{\nu}_1, \tilde{\nu}_2, \cdots, \tilde{\nu}_{card\{\mathcal{I}\}}\right]^T. \tag{101}$$

The corresponding KKT conditions are:

$$\frac{\partial \mathcal{L}}{\partial t} = \mathbf{1}^T\mathbf{u_2} - 1 = 0 \tag{102a}$$

$$\frac{\partial \mathcal{L}}{\partial \boldsymbol{\beta}} = \tilde{\delta}_0 \cdot 2\mathbf{Y}\boldsymbol{\beta} - \mathbf{D}^T\mathbf{F}^T\mathbf{u_2} = \mathbf{0} \tag{102b}$$

$$\boldsymbol{\beta}^T\mathbf{Y}\boldsymbol{\beta} - p_0 = 0 \tag{102c}$$

$$\tilde{\mu}_m\left(t - \mathbf{d}_m^T\boldsymbol{\beta}\right) = 0,\ \tilde{\mu}_m \ge 0,\ \forall \alpha_m^{\mathcal{O}} \in \mathcal{O} \tag{102d}$$

$$t - \mathbf{d}_n^T\boldsymbol{\beta} = 0,\ \forall \alpha_n^{\mathcal{I}} \in \mathcal{I} \tag{102e}$$

Then, by following a similar approach to Appendix B, the dual problem of $\mathcal{P}_{12}$ can be finally formulated into a QP optimization as well, shown as $\mathcal{P}_6$ in (32), which completes the proof. ■

APPENDIX F
PROOF FOR LEMMA 3

By comparing $\mathcal{P}_5$ with $\mathcal{P}_7$, we obtain that $\mathbf{Q} = \tilde{\mathbf{V}}^{-1}$ and $\mathbf{a} = \tilde{\mathbf{V}}\mathbf{1}$. Then, based on the expression in (90), we can obtain $\tilde{\mathbf{\Omega}}$ as a function of $\mathbf{q_E}$:

$$\begin{aligned}\tilde{\mathbf{\Omega}} &= \frac{1}{2\delta_0}\tilde{\mathbf{V}}^{-1}\left[\frac{1}{2}\left(\tilde{\mathbf{V}}-\mathbf{\Phi}\right)\mathbf{q_E}+\frac{\mathbf{a}}{c}\right]\\ &= \frac{1}{2\delta_0 c}\cdot\tilde{\mathbf{V}}^{-1}\mathbf{a}+\frac{1}{4\delta_0}\left(\mathbf{I}-\tilde{\mathbf{V}}^{-1}\mathbf{\Phi}\right)\mathbf{q_E}\\ &= \frac{1}{2\delta_0 c}\cdot\tilde{\mathbf{V}}^{-1}\tilde{\mathbf{V}}\mathbf{1}+\frac{1}{4\delta_0}\left(\mathbf{I}-\tilde{\mathbf{V}}^{-1}\mathbf{\Phi}\right)\mathbf{q_E}\\ &= \frac{1}{2\delta_0 c}\cdot\mathbf{1}+\frac{1}{4\delta_0}\left(\mathbf{I}-\tilde{\mathbf{V}}^{-1}\mathbf{\Phi}\right)\mathbf{q_E}. \end{aligned} \tag{103}$$

When all the dual variables are zero, $\mathbf{q_E} = \mathbf{0}$, and we see that the scaling value in $\tilde{\mathbf{\Omega}}$ for each data symbol is identical, which then leads to the ZF precoder. ■

APPENDIX G
PROOF FOR LEMMA 4

We calculate $\mathbf{1}^T\mathbf{u}$, which can be expressed as

$$\mathbf{1}^T\mathbf{u} = \frac{1}{2}\cdot\mathbf{1}^T\mathbf{Q}^{-1}\mathbf{q_E} - \frac{\mathbf{1}^T\mathbf{a}\mathbf{b}\mathbf{q_E}}{2c} + \frac{\mathbf{1}^T\mathbf{a}}{c}. \tag{104}$$

Based on the fact that $\mathbf{1}^T\mathbf{a} = c$, (104) is further equivalent to

$$\begin{aligned}\mathbf{1}^T\mathbf{u} &= \frac{1}{2}\cdot\mathbf{b}\mathbf{q_E} - \frac{c\cdot\mathbf{b}\mathbf{q_E}}{2c} + \frac{c}{c}\\ &= 1, \end{aligned} \tag{105}$$

which completes the proof. ■

ACKNOWLEDGMENT

The authors would like to thank Dr. Fan Liu for his valuable suggestions.

REFERENCES

[1] L. Zheng and D. N. C. Tse, "Diversity and multiplexing: A fundamental tradeoff in multiple-antenna channels," *IEEE Trans. Inf. Theory*, vol. 49, no. 5, pp. 1073–1096, May 2003.

[2] M. H. M. Costa, "Writing on dirty paper," *IEEE Trans. Inf. Theory*, vol. IT-29, no. 3, pp. 439–441, May 1983.

[3] L. Sun and M. Lei, "Quantized CSI-based tomlinson-harashima precoding in multiuser MIMO systems," *IEEE Trans. Wireless Commun.*, vol. 12, no. 3, pp. 1118–1126, Mar. 2013.

[4] B. M. Hochwald, C. B. Peel, and A. L. Swindlehurst, "A vector-perturbation technique for near-capacity multiantenna multiuser communication—Part II: Perturbation," *IEEE Trans. Commun.*, vol. 53, no. 3, pp. 537–544, Mar. 2005.

[5] A. Li and C. Masouros, "A constellation scaling approach to vector perturbation for adaptive modulation in MU-MIMO," *IEEE Wireless Commun. Lett.*, vol. 4, no. 3, pp. 289–292, Jun. 2015.

[6] A. Li and C. Masouros, "A two-stage vector perturbation scheme for adaptive modulation in downlink MU-MIMO," *IEEE Trans. Veh. Technol.*, vol. 65, no. 9, pp. 7785–7791, Sep. 2016.

[7] T. Haustein, C. von Helmolt, E. Jorswieck, V. Jungnickel, and V. Pohl, "Performance of MIMO systems with channel inversion," in *Proc. Veh. Technol. Conf. IEEE 55th Veh. Technol. Conf. VTC Spring*, vol. 1, Birmingham, AL, USA, 2002, pp. 35–39.

[8] C. B. Peel, B. M. Hochwald, and A. L. Swindlehurst, "A vector-perturbation technique for near-capacity multiantenna multiuser communication—Part I: Channel inversion and regularization," *IEEE Trans. Commun.*, vol. 53, no. 1, pp. 195–202, Jan. 2005.

[9] A. Wiesel, Y. C. Eldar, and S. Shamai (Shitz), "Linear precoding via conic optimization for fixed MIMO receivers," *IEEE Trans. Signal Process.*, vol. 54, no. 1, pp. 161–176, Jan. 2006.

[10] M. F. Hanif, L.-N. Tran, A. Tolli, and M. Juntti, "Computationally efficient robust beamforming for SINR balancing in multicell downlink with applications to large antenna array systems," *IEEE Trans. Commun.*, vol. 62, no. 6, pp. 1908–1920, Jun. 2014.

[11] F. Wang, X. Wang, and Y. Zhu, "Transmit beamforming for multiuser downlink with per-antenna power constraints," in *Proc. IEEE Int. Conf. Commun. (ICC)*, Sydney, NSW, Australia, Jun. 2014, pp. 4692–4697.

[12] M. Schubert and H. Boche, "Solution of the multiuser downlink beamforming problem with individual SINR constraints," *IEEE Trans. Veh. Technol.*, vol. 53, no. 1, pp. 18–28, Jan. 2004.

[13] M. Bengtsson and B. Ottersten, "Optimal and suboptimal transmit beamforming," in *Handbook of Antennas in Wireless Communications*, 1st ed. Boca Raton, FL, USA: CRC Press, Aug. 2001.

[14] N. D. Sidiropoulos, T. N. Davidson, and Z.-Q. Luo, "Transmit beamforming for physical-layer multicasting," *IEEE Trans. Signal Process.*, vol. 54, no. 6, pp. 2239–2251, Jun. 2006.

[15] E. Karipidis, N. D. Sidiropoulos, and Z.-Q. Luo, "Quality of service and max-min fair transmit beamforming to multiple cochannel multicast groups," *IEEE Trans. Signal Process.*, vol. 56, no. 3, pp. 1268–1279, Mar. 2008.

[16] C. Masouros, T. Ratnarajah, M. Sellathurai, C. B. Papadias, and A. K. Shukla, "Known interference in the cellular downlink: A performance limiting factor or a source of green signal power?" *IEEE Commun. Mag.*, vol. 51, no. 10, pp. 162–171, Oct. 2013.

[17] G. Zheng, I. Krikidis, C. Masouros, S. Timotheou, D.-A. Toumpakaris, and Z. Ding, "Rethinking the role of interference in wireless networks," *IEEE Commun. Mag.*, vol. 52, no. 11, pp. 152–158, Nov. 2014.

[18] A. Li *et al.*, "A tutorial on interference exploitation via symbol-level precoding: Overview, state-of-the-art and future directions," *IEEE Commun. Surveys Tuts.*, vol. 22, no. 2, pp. 796–839, 2nd Quart., 2020.

[19] C. Masouros and E. Alsusa, "A novel transmitter-based selective-precoding technique for DS/CDMA systems," *IEEE Signal Process. Lett.*, vol. 14, no. 9, pp. 637–640, Sep. 2007.

[20] C. Masouros and E. Alsusa, "Dynamic linear precoding for the exploitation of known interference in MIMO broadcast systems," *IEEE Trans. Wireless Commun.*, vol. 8, no. 3, pp. 1396–1401, Mar. 2009.

[21] C. Masouros, "Correlation rotation linear precoding for MIMO broadcast communications," *IEEE Trans. Signal Process.*, vol. 59, no. 1, pp. 252–262, Jan. 2011.

[22] C. Masouros, M. Sellathurai, and T. Ratnarajah, "Vector perturbation based on symbol scaling for limited feedback MISO downlinks," *IEEE Trans. Signal Process.*, vol. 62, no. 3, pp. 562–571, Feb. 2014.

[23] C. Masouros and G. Zheng, "Exploiting known interference as green signal power for downlink beamforming optimization," *IEEE Trans. Signal Process.*, vol. 63, no. 14, pp. 3628–3640, Jul. 2015.

[24] M. Alodeh, S. Chatzinotas, and B. Ottersten, "Constructive multiuser interference in symbol level precoding for the MISO downlink channel," *IEEE Trans. Signal Process.*, vol. 63, no. 9, pp. 2239–2252, May 2015.

[25] M. Alodeh, S. Chatzinotas, and B. Ottersten, "Energy-efficient symbol-level precoding in multiuser MISO based on relaxed detection region," *IEEE Trans. Wireless Commun.*, vol. 15, no. 5, pp. 3755–3767, May 2016.

[26] A. Li and C. Masouros, "Exploiting constructive mutual coupling in P2P MIMO by analog-digital phase alignment," *IEEE Trans. Wireless Commun.*, vol. 16, no. 3, pp. 1948–1962, Mar. 2017.

[27] M. T. Kabir, M. R. A. Khandaker, and C. Masouros, "Interference exploitation in full-duplex communications: Trading interference power for both uplink and downlink power savings," *IEEE Trans. Wireless Commun.*, vol. 17, no. 12, pp. 8314–8329, Dec. 2018.

[28] M. Alodeh, S. Chatzinotas, and B. Ottersten, "Symbol-level multiuser MISO precoding for multi-level adaptive modulation," *IEEE Trans. Wireless Commun.*, vol. 16, no. 8, pp. 5511–5524, Aug. 2017.

[29] A. Li, C. Masouros, F. Liu, and A. L. Swindlehurst, "Massive MIMO 1-Bit DAC transmission: A low-complexity symbol scaling approach," *IEEE Trans. Wireless Commun.*, vol. 17, no. 11, pp. 7559–7575, Nov. 2018.

[30] F. Liu, C. Masouros, A. Li, T. Ratnarajah, and J. Zhou, "MIMO radar and cellular coexistence: A power-efficient approach enabled by interference exploitation," *IEEE Trans. Signal Process.*, vol. 66, no. 14, pp. 3681–3695, Jul. 2018.

[31] H. Jedda, A. Mezghani, A. L. Swindlehurst, and J. A. Nossek, "Quantized constant envelope precoding with PSK and QAM signaling," *IEEE Trans. Wireless Commun.*, vol. 17, no. 12, pp. 8022–8034, Dec. 2018.

[32] A. Li, F. Liu, C. Masouros, Y. Li, and B. Vucetic, "Interference exploitation 1-Bit massive MIMO precoding: A partial branch-and-bound solution with near-optimal performance," *IEEE Trans. Wireless Commun.*, vol. 19, no. 5, pp. 3474–3489, May 2020.

[33] A. Li, C. Masouros, A. Lee Swindlehurst, and W. Yu, "1-bit massive MIMO transmission: Embracing interference with symbol-level precoding," 2020, *arXiv:2007.13950*. [Online]. Available: http://arxiv.org/abs/2007.13950

[34] Y. Fan, A. Li, X. Liao, and V. C. M. Leung, "Secure interference exploitation precoding in MISO wiretap channel: Destructive region redefinition with efficient solutions," *IEEE Trans. Inf. Forensics Security*, vol. 16, pp. 402–417, Jul. 2021.

[35] F. Liu, C. Masouros, P. V. Amadori, and H. Sun, "An efficient manifold algorithm for constructive interference based constant envelope precoding," *IEEE Signal Process. Lett.*, vol. 24, no. 10, pp. 1542–1546, Oct. 2017.

[36] A. Li and C. Masouros, "Interference exploitation precoding made practical: Optimal closed-form solutions for PSK modulations," *IEEE Trans. Wireless Commun.*, vol. 17, no. 11, pp. 7661–7676, Sep. 2018.

[37] A. Salem, C. Masouros, and K.-K. Wong, "Sum rate and fairness analysis for the MU-MIMO downlink under PSK signalling: Interference suppression vs exploitation," *IEEE Trans. Commun.*, vol. 67, no. 9, pp. 6085–6098, Sep. 2019.

[38] A. Salem, C. Masouros, and B. Clerckx, "Rate splitting with finite constellations: The benefits of interference exploitation vs suppression," 2019, *arXiv:1907.08457*. [Online]. Available: http://arxiv.org/abs/1907.08457

[39] M. Alodeh, S. Chatzinotas, and B. Ottersten, "Constructive interference through symbol level precoding for multi-level modulation," in *Proc. IEEE Global Commun. Conf. (GLOBECOM)*, San Diego, CA, USA, Dec. 2015, pp. 1–6.

[40] A. Li, C. Masouros, Y. Li, and B. Vucetic, "Interference exploitation precoding for multi-level modulations," in *Proc. IEEE Int. Conf. Acoust., Speech Signal Process. (ICASSP)*, Brighton, U.K., May 2019, pp. 4679–4683.

[41] A. Ben-Israel and T. N. E. Greville, *Generalized Inverses: Theory and Applications*, 2nd ed. New York, NY, USA: Springer, 2003.

[42] L. Vandenberghe and S. Boyd, *Convex Optimization*. Cambridge, U.K.: Cambridge Univ. Press, 2004.

Ang Li (Member, IEEE) received the Ph.D. degree from the Communications and Information Systems research group, Department of Electrical and Electronic Engineering, University College London, U.K., in 2018. He was a Post-Doctoral Research Associate with the School of Electrical and Information Engineering, The University of Sydney, Sydney, Australia, from May 2018 to February 2020. In March 2020, he joined Xi'an Jiaotong University, Xi'an, China, where he is currently a Professor with the School of Information and Communications Engineering, Faculty of Electronic and Information Engineering. His research areas include precoding and signal processing techniques for MIMO and massive MIMO systems, with focus on interference exploitation precoding and its applications. He was a recipient of the Exemplary Reviewer for IEEE COMMUNICATIONS LETTERS and IEEE TRANSACTIONS ON COMMUNICATIONS in 2017 and 2019. He has served as the Co-Organizer and Co-Chair for the IEEE ICASSP 2020 Special Session on "Hardware-Efficient Large-Scale Antenna Arrays: The Stage for Symbol-Level Precoding."

Christos Masouros (Senior Member, IEEE) received the Diploma degree in electrical and computer engineering from the University of Patras, Greece, in 2004, and the M.Sc. (by research) and Ph.D. degrees in electrical and electronic engineering from The University of Manchester, U.K., in 2006 and 2009, respectively.

In 2008, he was a Research Intern with Philips Research Labs, U.K. From 2009 to 2010, he was a Research Associate with The University of Manchester, and a Research Fellow with Queen's University Belfast from 2010 to 2012. In 2012, he joined University College London as a Lecturer. He has held a Royal Academy of Engineering Research Fellowship from 2011 to 2016. He is currently a Full Professor with the Information and Communication Engineering research group, Department of Electrical and Electronic Engineering, and affiliated with the Institute for Communications and Connected Systems, University College London. His research interests include the field of wireless communications and signal processing, with particular focus on green communications, large scale antenna systems, communications and radar co-existence, and interference mitigation techniques for MIMO and multi-carrier communications. He was a recipient of the Best Paper Awards in the IEEE GLOBECOM 2015 and IEEE WCNC 2019 conferences, and has been recognized as an Exemplary Editor of IEEE COMMUNICATIONS LETTERS, and as an Exemplary Reviewer of IEEE TRANSACTIONS ON COMMUNICATIONS. He is currently the Chair of the IEEE Special Interest Group on Energy Harvesting and an Elected Member of the EURASIP SAT Committee on Signal Processing for Communications and Networking. He is an Editor of IEEE TRANSACTIONS ON COMMUNICATIONS, IEEE TRANSACTIONS ON WIRELESS COMMUNICATIONS, IEEE OPEN JOURNAL OF SIGNAL PROCESSING, and an Editor-at-Large for IEEE OPEN JOURNAL OF THE COMMUNICATIONS SOCIETY. He has been an Associate Editor of IEEE COMMUNICATIONS LETTERS, and a Guest Editor of IEEE JOURNAL OF SELECTED TOPICS IN SIGNAL PROCESSING issues "Exploiting Interference towards Energy Efficient and Secure Wireless Communications" and "Hybrid Analog/Digital Signal Processing for Hardware-Efficient Large Scale Antenna Arrays."

Branka Vucetic (Life Fellow, IEEE) is an internationally recognized expert in coding theory and its applications in wireless engineering. She has held various research and academic positions in the U.K., Yugoslavia, and Australia, and she has been with the School of Electrical and Information Engineering, Sydney University, since 1986, where she is currently a Laureate Professor and the Director of the Centre of Excellence for the IoT and Telecommunications. She has published four books and more than 300 papers in telecommunications journals and conference proceedings. Her research interests include wireless communications, digital communication theory, error control coding, and multi-user detection.

She is a fellow of the Australian Academy of Science (AAS), the Australian Academy of Technological Sciences and Engineering (ATSE). She was a recipient of the Chinese Government Friendship Award, and a former Editor of IEEE TRANSACTIONS ON COMMUNICATIONS. In the last several years, she has managed several projects related to wireless communications networks development, addressing the issues like interference cancellation, multiple antenna signal processing and coding, and multiple access technologies.

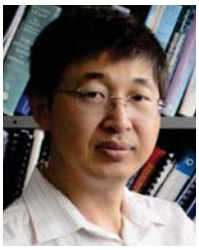

Yonghui Li (Fellow, IEEE) received the Ph.D. degree from the Beijing University of Aeronautics and Astronautics in November 2002. From 1999 to 2003, he was affiliated with LinkAir Communication Inc., where he held a position of project manager with responsibility for the design of physical layer solutions for the LAS-CDMA system. Since 2003, he has been with the Centre of Excellence in Telecommunications, The University of Sydney, Australia, where he is currently a Professor with the School of Electrical and Information Engineering. He was a recipient of the Australian Queen Elizabeth II Fellowship in 2008, and the Australian Future Fellowship in 2012. His current research interests include the area of wireless communications, with a particular focus on MIMO, millimeter wave communications, machine to machine communications, coding techniques, and cooperative communications. He holds a number of patents granted and pending in these fields. He received the best paper awards from IEEE International Conference on Communications (ICC) 2014, IEEE PIMRC 2017, and IEEE Wireless Days Conferences (WD) 2014. He is currently an Editor of IEEE TRANSACTIONS ON COMMUNICATIONS and IEEE TRANSACTIONS ON VEHICULAR TECHNOLOGY. He also served as a guest editor for several special issues of IEEE journals, such as the IEEE JOURNAL ON SELECTED AREAS IN COMMUNICATIONS Special Issue on Millimeter Wave Communications.

A. Lee Swindlehurst (Fellow, IEEE) received the B.S. and M.S. degrees in electrical engineering from Brigham Young University (BYU) in 1985 and 1986, respectively, and the Ph.D. degree in electrical engineering from Stanford University in 1991. He was with the Department of Electrical and Computer Engineering, BYU, from 1990 to 2007, where he served as the Department Chair from 2003 to 2006. From 1996 to 1997, he held a joint appointment as a Visiting Scholar at Uppsala University and the Royal Institute of Technology, Sweden. From 2006 to 2007, he was on leave working as the Vice President of Research for ArrayComm LLC, San Jose, CA, USA. Since 2007, he has been a Professor with the Electrical Engineering and Computer Science Department, University of California at Irvine, where he served as the Associate Dean for Research and Graduate Studies in the Samueli School of Engineering from 2013 to 2016. From 2014 to 2017, he was also a Hans Fischer Senior Fellow of the Institute for Advanced Studies, Technical University of Munich. His research focuses on array signal processing for radar, wireless communications, and biomedical applications, and he has over 300 publications in these areas. He received the 2000 IEEE W. R. G. Baker Prize Paper Award, the 2006 IEEE Communications Society Stephen O. Rice Prize in the Field of Communication Theory, the 2006 and 2010 IEEE Signal Processing Society's Best Paper Awards, and the 2017 IEEE Signal Processing Society Donald G. Fink Overview Paper Award. He was the inaugural Editor-in-Chief of IEEE JOURNAL OF SELECTED TOPICS IN SIGNAL PROCESSING.